JCI insight

microRNA-33 deficiency in macrophages enhances autophagy, improves mitochondrial homeostasis, and protects against lung fibrosis

Farida Ahangari, … , Carlos Fernandez-Hernando, Naftali Kaminski

JCI Insight. 2023. https://doi.org/10.1172/jci.insight.158100.

Research In-Press Preview Metabolism Pulmonology

Graphical abstract

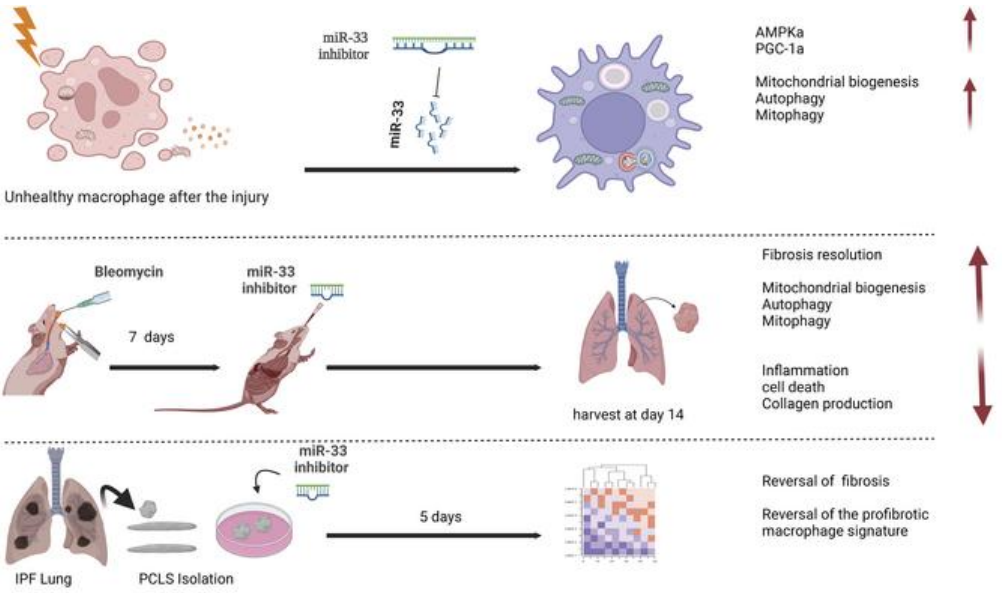

Find the latest version:

https://jci.me/158100/pdf

microRNA-33 Deficiency in Macrophages Enhances Autophagy, Improves Mitochondrial Homeostasis and Protects Against Lung Fibrosis

Authors:
Farida Ahangari[1]†, Nathan L. Price[2,3]†, Shipra Malik[4], Maurizio Chioccioli[1], Thomas Bärnthaler[1,5], Taylor Adams[1], Jooyoung Kim[1], Sai Pallavi Pradeep[4], Shuizi Ding[1], Carlos Cosmos Jr.[1], Kadi-Ann S. Rose[1], John E. Mcdonough[1], Nachelle R. Aurelien[1,6], Gabriel Ibarra[1,7], Norihito Omote[1], Jonas C. Schupp[1], Giuseppe Deluliis[1], Julian Villalba Nunez[8], Lokesh Sharma[1], Changwan Ryu[1], Charles S. Dela Cruz[1], Xinran Liu[9], Antje Prasse[10], Ivan Rosas[8,11], Raman Bahal[4], Carlos Fernández-Hernando[2]†*, Naftali Kaminski[1]†*

Affiliations:

[1] Section of Pulmonary, Critical care and Sleep Medicine, Yale University School of Medicine; New Haven, CT, USA.

[2] Vascular Biology and Therapeutics Program, Yale Center for Molecular and System Metabolism, Department of Comparative Medicine, and Department of Pathology; Yale University School of Medicine, New Haven, CT, USA,

[3] Experimental Gerontology Section, Translational Gerontology Branch, National Institute on Aging, National Institutes of Health, Baltimore, MD, USA

[4] Department of Pharmaceutical Sciences, School of Pharmacy, University of Connecticut; Storrs, CT, USA

[5] Division of Pharmacology, Otto Loewi Research Center, Medical University of Graz, Austria

[6] Department of Internal Medicine, Weill Cornell Hospital Medicine, New York, NY, USA

[7] Life Span Medical Group, Department of Internal Medicine, Rhode Island Hospital, Providence, RI, USA

[8] Division of Pulmonary and Critical Care Medicine, Brigham and Women's Hospital, Harvard Medical School, Boston, MA, USA.

[9] Center for Cellular and Molecular Imaging, Department of Cell Biology, Yale School of Medicine, New Haven, CT, USA

[10] Department of Medicine, Baylor College of Medicine, Houston, TX, USA

[11] Department of Pneumology, University of Hannover, Fraunhofer Institute for Toxicology and Experimental Medicine ITEM; DZL BREATH, Hannover, Germany

† "These authors contributed equally to this work."

*** Corresponding authors**:

Naftali Kaminski, MD

Pulmonary, Critical Care and Sleep Medicine Section, Department of Internal Medicine, Yale University School of Medicine, New Haven, Connecticut, USA, 06510

Tel: 2037374612

Fax: 2037853826

E-mail: naftali.kaminski@yale.edu

Carlos Fernández-Hernando, PhD

Vascular Biology and Therapeutics Program, Yale Center for Molecular and System Metabolism, Department of Comparative Medicine, and Department of Pathology, Yale University School of Medicine, New Haven, CT, USA, 06510

Tel: 2037374516

Fax: 2037372290

E-mail: carlos.fernandez@yale.edu

ABSTRACT

Idiopathic pulmonary fibrosis (IPF) is a progressive and ultimately fatal disease. Recent findings have shown a marked metabolic reprogramming associated with changes in mitochondrial homeostasis and autophagy during pulmonary fibrosis. The microRNA-33 (miR-33) family of microRNAs (miRNAs) encoded within the introns of *SREBP* (sterol regulatory element binding protein) genes are master regulators of sterol and fatty acid (FA) metabolism. miR-33 controls macrophage immuno-metabolic response and enhances mitochondrial biogenesis, FA oxidation, and cholesterol efflux. Here, we show that miR-33 levels are increased in Broncho Alveolar Lavage (BAL) cells isolated from IPF patients compared to healthy controls. We demonstrate that specific genetic ablation of *miR-33* in macrophages protects against bleomycin-induced pulmonary fibrosis. The absence of miR-33 in macrophages improves mitochondrial homeostasis and increases autophagy while decreasing inflammatory response after bleomycin injury. Notably, pharmacological inhibition of miR-33 in macrophages via administration of anti-miR-33 Peptide Nucleic Acids (PNA-33) attenuates fibrosis in different *in vivo* and *ex vivo* mice and human models of pulmonary fibrosis. Together, these studies elucidate a major role of miR-33 in macrophages in the regulation of pulmonary fibrosis and uncover a novel therapeutic approach to treat this disease.

INTRODUCTION

Pulmonary Fibrosis (PF) is a chronic, fatal and progressive disease characterized by an aberrant wound healing caused by repetitive alveolar epithelial cell injury and excessive deposition of extracellular matrix proteins in the interstitial space of the lung (1). There are two main types of pulmonary fibrosis: 1) with unknown etiology (Idiopathic) and 2) secondary to autoimmunity, exposure to environmental factors such as foreign antigens, toxins, chemical warfare, radiation, or viral infection. The median survival of Idiopathic Pulmonary Fibrosis (IPF) is 3-5 years after initial diagnosis and its incidence continues to rise (1-3). Two FDA-approved drugs, pirfenidone, and nintedanib slow disease progression, but have no effect on patient symptoms or quality of life, and the only curative treatment for pulmonary fibrosis is lung transplantation (4).

A growing body of evidence supports the role of macrophages in the pathogenesis of pulmonary fibrosis. Although many cell types are involved in tissue repair, macrophages have been shown to exhibit critical regulatory activity at all stages of repair and fibrosis (5). Consequently, because macrophages represent potentially important therapeutic targets, there has been a great deal of interest over the past few years in deciphering the contributions of the different macrophage populations that control the initiation, maintenance, and resolution of wound healing responses (5). Lung macrophages are a critical component of the pulmonary fibrotic response in mice and humans, as has been most recently demonstrated by studies that applied single cell RNA sequencing technologies (6, 7), and numerous mechanistic studies (8-10). In the past decade, there has been increased recognition of the roles of aging, innate immunity, metabolic reprogramming, and mitochondrial dysfunction in PF (10-13), and it has been shown that mitochondria in Alveolar Macrophages (AM)s from IPF patients have prominent morphological and transcriptional defects

(14). Taken together manipulation of these macrophages and their metabolic programs may present an attractive therapeutic strategy to treat pulmonary fibrosis (15).

The miR-33 family (*miR-33a* and *miR-33b*) of intronic miRNAs has been shown to control lipid metabolism, as well as cellular energy status and mitochondrial function (16-23). Inhibition of endogenous miR-33 in macrophages promotes mitochondrial biogenesis and efficient production of adenosine triphosphate (ATP) (16, 24). miR-33 sustains cardiac fibrosis and remodeling by preserving lipid raft cholesterol content and controlling proliferation in cardiac fibroblasts (25). Loss or inhibition of miR-33 is protective in multiple models of kidney dysfunction, which may be in part due to a reduction of the repression of fatty acid oxidation (FAO) in fibrotic kidneys and reduced lipid accumulation (26). Additionally, hepatic miR-33 deficiency has been demonstrated to protect against liver fibrosis and improve metabolic function in mice fed a high fat diet (27). However, the regulatory role of miR-33 in the context of lung fibrosis has not been elucidated yet.

In this study, we discovered that miR-33 regulates the immuno-metabolic responses of macrophages during PF. Most importantly, we demonstrate that miR-33 therapeutic silencing in lung macrophages attenuates the progression of lung fibrosis in *in vivo* and *ex vivo* models. These findings may overcome one of the main problems in treating lung-related disorders with RNA-based medicines, which is the lack of targeted miRNA delivery technology to minimize off-target effects and improve the safety of miRNAs *in vivo* (28).

RESULTS

miR-33 levels are increased in monocytes/macrophages isolated from Broncho Alveolar Lavages (BAL) and lungs of IPF patients compared to healthy controls:

We evaluated the level of miR-33 in BAL cells, obtained from 62 well-characterized patients with IPF and 10 age-matched healthy controls **(Table S1)**. This analysis revealed that miR-33 is significantly increased in IPF cells compared to controls (fold change; +2.5, P-value=0.0024) **(Fig. 1A)**. Since more than 90% of BAL cells are immune cells, we aimed to evaluate miR-33 levels in the immune cells of the human lungs. We isolated $CD45^+$ cells from the lungs of the patients with IPF (n=9) **(Table S2)** and identified a significant increase in miR-33 levels (P-value=0.023) in IPF $CD45^+$ cells compared to controls (n=4) **(Fig. 1B)**. Interestingly, the expression of miR-33 in IPF $CD45^-$ populations were significantly lower than controls (P-value≤0.001), which suggested a potentially important regulatory role for miR-33 in immune cells and perhaps monocyte/macrophage populations in IPF. To expand our analysis and provide a better understanding of miR-33 regulation in human, we assessed indicators of miR-33 activity in publicly available gene expression lung datasets. We identified miR-33 target genes in two gene expression datasets, one from lung tissue (GSE47460) and one from BAL (GSE70866). As a single gene's expression is a poor correlate for miRNA activity, we determined overall miRNA activity by analyzing all target genes using Gene Set Variation Analysis (GSVA). This analysis revealed that miR-33-5p target gene expression is significantly decreased in both IPF BAL (5p; P-value=0.000187,3p; P-value=2.57e-05) **(Fig. 1C)** and IPF lung tissues (5p; P-value=2.64e-06) **(Fig. 1D)**. Targets of the 3p strand of the microRNA were significantly decreased in BAL but not in lung tissue **(Fig. S1A** and **B).**

Myeloid-specific miR-33 knockout mice are protected against bleomycin-induced Pulmonary Fibrosis:

To directly test the immune cell specific role of miR-33, we generated myeloid-specific miR-33 knockout (KO) mice (*LysM^{CRE+}miR-33$^{LOX/LOX}$*, *miR-33$^{M/M}$-/-),* and appropriate controls

LysM^{CRE}-*miR-33*$^{LOX/LOX}$, *miR-33*$^{M/M}$+/+) and subjected to a bleomycin-induced PF model. The evaluation of miR-33 levels in BAL Alveolar Macrophages (AM), as well as the total lungs of these mice, confirmed the absence of miR-33 in macrophages, and that bleomycin administration increases the levels of miR-33 in control mice compared to the saline-treated group **(Fig. 2A** and Fig **S2A)**. *miR-33*$^{M/M}$-/- mice were protected from bleomycin-induced lung fibrosis as indicated by a reduction in collagen content, measured by hydroxyproline assay (fold change; -2, P≤0.0001), **(Fig. 2B)**, and expression of profibrotic genes including *Col1a1* and *Acta2* (fold change; -2.5, P≤0.0001), **(Fig. 2C-D)**. The histological evaluations using Masson-Trichrome staining of lung tissues confirmed these findings **(Fig. 2E-F)**. Next, we evaluated the inflammatory response in these mice via the measurements of BAL cell recovery and the cytokines level after the bleomycin injury. BAL total cell numbers as well as macrophage and lymphocyte cell numbers were significantly increased in the control mice with bleomycin treatment and largely ameliorated in the absence of miR-33 (**Fig. 2G)**. Measurements of cytokine panels in the BAL isolated from these mice revealed that many of the inflammatory markers including TNFα, IL-12p70, IL-2, INF-γ, KC-GRO, IL10, IL-13, and IL-4 are decreased in the absence of miR-33 after bleomycin injury **(Fig. 2H-O)**.

We investigated the expression of miR-33 target transcripts relevant to mitochondrial homeostasis in these samples and identified numerous targets, including peroxisome proliferator-activated receptor gamma coactivator-1α (*Pgc-1α*, *Ppargc1a*), Carnitine O-Octanoyltransferase *(Crot*), Carnitine Palmitoyltransferase-*1 α* (*Cpt1α*), and ATP Binding Cassette Subfamily A Member1 (*Abca1*), with increased expression in the absence of miR-33 at baseline and after bleomycin exposure **(Fig. 2P-S)**. The same pattern of changes was observed in the level of Sirtuin3 (*Sirt3*) expression **(Fig. 2T)**, which could be secondary to other effects induced by the absence of

miR-33. As expected, the administration of bleomycin reduces the expression of some of these genes in the control mice **(Fig. 2P-T)**. The expression of the miR-33 host gene, Sterol Regulatory Element Binding Transcription Factor 2 (*Srebp-2*) was increased in the lungs of the *miR-33*$^{M/M}$*-/-* mice **(Fig. S2B** and **S2C)**. Together, this data revealed the protective effect of macrophage-specific miR-33 ablation in the bleomycin model of PF in mice and suggested that this effect could be via alterations in the expression of target genes relevant to mitochondrial function.

Pharmacological inhibition of miR-33 in lung macrophages protects against bleomycin in *in vivo* murine model of PF:

Peptide Nucleic Acids (PNAs) are synthetic analogs of DNA comprised of nucleobases that are connected to a pseudo-peptide backbone which imparts resistance to nuclease enzymes and considerably increases stability and half-life (29, 30). We generated and assessed the efficacy of anti-miR-33 PNA (PNA-33) as a cell-specific inhibitor for miR-33. Our results showed that PNA-33 binds specifically to well-established miR-33 target transcripts by gel shift assay **(Fig. 3A)**. In prior studies, we optimized the protocol for the preparation of PNA conjugates containing the fluorophore TAMRA (31). We administered PNA-33 TAMRA conjugated anti-miR in WT mice via intravenous (IV) route and confirmed the accumulation of the compound in lung macrophages 24 hours after injection using a two-photon microscopy imaging system **(Fig. 3B)**. Next, we administered PNA-33 and scrambled control in WT mice via an intranasal (IN) route, which is the most efficient method for direct delivery to the lung and isolated lungs and alveolar macrophages (AM) at different time points. As shown in **Figure 3C**, miR-33 levels were dramatically decreased, specifically in AM after PNA-33 administration, and remained at low levels even 5 days after a single administration of PNA-33 **(Fig. 3C)**. After confirming the efficacy of PNA-33 in delivering and antagonizing miR-33 in macrophages, we tested whether therapeutic

115 silencing of miR-33 using PNA-33 protects against bleomycin-induced PF in mice. Notably, we
116 found that intranasal administration of PNA-33 markedly reduces lung fibrosis as indicated by a
117 significant decrease in collagen content and fibrogenic gene expression (*Col1a1* and *Acta2*)
118 compared to mice treated with scrambled control **(Fig. 3D-F)**. Histological assessments in lung
119 sections via quantifications of the collagen accumulations in Mason Trichrome staining confirmed
120 the fibro-protective effects of PNA-33 in this mice model **(Fig. 3G** and **H)**. Consistent with what
121 we observed in *miR-33*$^{M/M}$*-/-* mice, the expressions of mitochondrial-related miR-33 target genes
122 (*Pgc-1α*) and (*Abca1*) were increased in response to PNA-33 treatment **(Fig. 3I** and **J)**.

123 Collectively, our results demonstrated that macrophage-specific deletion and
124 pharmacological inhibition of miR-33 in the lung protect against bleomycin-induced PF in *in vivo*
125 model.

126 **The absence of miR-33 in macrophages improves mitochondrial homeostasis at baseline and**
127 **after bleomycin injury:**

128 To understand the mechanism behind the fibro-protective effects of miR-33 inhibition and
129 to confirm its regulatory role in the expression of genes associated with mitochondrial biogenesis
130 and metabolism in macrophages, we tested primary mice AM in an *ex vivo* system. Inhibition of
131 miR-33 using a miR-33 antagomir with or without bleomycin treatment revealed a significant
132 increase in the expression of miR-33 target genes *Pgc-1α*, *Abca1,* and *Sirt3* expression indicating
133 a role of miR-33 in regulating key mitochondrial pathways **(Fig. 4A-D)**. To further explore the
134 regulatory role of miR-33 in mitochondrial homeostasis in macrophages, we measured
135 mitochondrial function in primary AM isolated from myeloid-specific miR-33 knockout mice by
136 Seahorse XF96 Extracellular Flux Analyzer. As expected, mitochondrial activity in AM of control
137 mice was very limited at baseline and after bleomycin injury. Interestingly, we found a dramatic

increase in mitochondrial function, as indicated by a significant increase in Oxygen Consumption Rate (OCR, pmol/min) and Extracellular Acidification Rate (ECAR, pmpH/min) (Fold=+3), in the *miR-33$^{M/M}$-/-* AM compared to control AM at baseline and after bleomycin exposure **(Fig. 4E-H)**.

Emerging evidence suggests that the examination of circulating mitochondrial DNA (mtDNA) could be a mechanism-based prognostic biomarker of PF (32). Thus, we evaluated mtDNA in the extracellular fraction of the BAL isolated from *miR-33$^{M/M}$-/-* and controls post bleomycin injury (32). Notably, we observed a significant increase in mtDNA content in control mice after bleomycin injury, which is markedly decreased in the absence of miR-33 in macrophages after bleomycin or even at baseline **(Fig. 4I)**. As we observed an improved oxygenation rate and decreased extracellular mitochondrial DNA in the BAL, we hypothesized that miR-33 deficiency improves mitochondrial stability. To evaluate the effect of miR-33 inhibition on structural alterations in the mitochondria in the lung, we performed Transmission Electron Microscopy (TEM) imaging analyses on lung tissues as well as AM isolated from control and *miR-33$^{M/M}$-/-* mice **(Fig. 4J-M)**. Ultrastructural qualitative and quantitative analysis revealed that the mitochondria in macrophages from control mice after bleomycin injury were dysmorphic and contained disorganized cristae **(Fig. 4L, N,** and **O**). These deleterious morphological mitochondrial alterations were partially prevented in macrophages from *miR-33$^{M/M}$-/-* mice. Detailed morphometric analysis of macrophages from *miR-33$^{M/M}$-/-* mice demonstrated a significant improvement in the mitochondrial structure as well as an increase in the mitochondrial number/area at the baseline and strikingly after bleomycin exposure **(Fig. 4M, N** and **O)**.

The absence of miR-33 in macrophages induces autophagy after bleomycin injury:

We extended our investigation by further evaluating the TEM images acquired from the lung tissues and AM from *miR-33$^{M/M}$-/-* mice after bleomycin exposure. In addition to the

improvement in mitochondrial structure, we found a dramatic enhancement in autophagy as visualized by an increase in autophagosome contents, specifically in the *miR-33$^{M/M}$-/-* macrophages after bleomycin **(Fig. 5A)**. Given that AMP-activated protein kinase Alpha (*AMPK-α*) and *PGC-1α* are well-established miR-33 target genes, relevant to mitochondrial homeostasis and autophagy, we evaluated their protein expressions in these mice. Western blot analysis of the lung tissues revealed an increase in the expression of Phospho-AMPK-α and PGC-1α, in *miR-33$^{M/M}$-/-* mice at baseline and after bleomycin exposure compared to control mice **(Fig. 5B)**. To confirm the relationship between the absence of miR-33 in macrophages and autophagy, we also evaluated AM after the inhibition of miR-33 using an antagomir and found an increase in phospho-AMPK-α as well as LC3A/B and P62 (also known as SQSTM1) expression in these cells compared to the scrambled control **(Fig. 5C)**. Immunohistochemistry (IHC) staining in lung tissues isolated from *miR-33$^{M/M}$-/-* mice showed a significant increase in LC3A/B **(Fig. 5D** and **E)** and P62 **(Fig. 5F** and **G)** positive cells in these mice compared to controls after bleomycin injury. Co-IHC of LC3A/B and P62 along with F4/80 (a marker of macrophages in the lung) identified co-localization of F4/80 with LC3A/B and P62n in the lungs of *miR-33$^{M/M}$-/-* mice after bleomycin **(Fig. S3A-C)**.

miR-33 deficiency in macrophages induces mitophagy in response to injury:

Mitophagy is a quality control mechanism that could be regulated independently of the signals that govern autophagy (33), therefore we sought to study the effects of miR-33 inhibition on mitophagy after bleomycin injury. To this end, we isolated primary AM from WT mice and treated them with PNA-33 or scramble control after bleomycin injury. Confocal imaging analysis demonstrated that miR-33 inhibition markedly induces mitophagy at baseline and after bleomycin injury in macrophages **(Fig. 6A** and **B).** We next evaluated *Pink1* and *Parkin* gene expressions and

found a significant increase in the expression of these two critical regulators of mitophagy in the miR-33 deficient AM after bleomycin treatment **(Fig. 6C** and **D)**. Notably, mitophagy was also increased in CD45+ cells isolated from IPF patients after miR-33 inhibition **(Fig. 6E)**, which further confirmed the concordance of this finding between human and mice lung fibrosis.

Taken together, these data demonstrate the fibro-protective role of macrophage miR-33 ablation via improving mitochondrial function and structure at baseline and after bleomycin injury as well as increasing autophagy/mitophagy in these cells.

Targeted inhibition of miR-33 in macrophages alters the proinflammatory/anti-inflammatory gene expression profile:

Given the importance of macrophages in the Th1/Th2 paradigm in PF, we assessed how miR-33 inhibition influenced macrophage immune responses. We isolated AM from WT mice and skewed them toward M1 (using INF-γ plus LPS) or M2 (using IL-13) after miR-33 inhibition using PNA-33. As was expected INF-γ induced the expression of pro-inflammatory genes including *Arg1*(Arginase 1), *Chi3L1*(chitinase 3 like 1), and *IL-12*, and interestingly the expression of all these profibrotic markers decreased after miR-33 inhibition **(Fig. 6F-H)**. Conversely, INF-γ decreased the expression of *Sirt-1*, which was reversed after PNA-33 treatment **(Fig. 6I)**.

M2 alternative activated macrophages gene expression analysis revealed that miR-33 ablation reversed the IL-13 induced *YM1* (Chitinase like 3, *Chil3*) levels in these cells **(Fig. 6J).** Notably, miR-33 inhibition of IL-13 treated cells increased the expression of *Abca1* and *Ppar-γ* **(Fig. 6K and L).**

This experiment suggests a potential regulatory role for miR-33 in skewing proinflammatory/anti-inflammatory macrophages which may be beneficial in fibrosis resolution.

Lack of miR-33 in myeloid cells improves mitochondrial homeostasis and decreases cell death in Alveolar Type II cells after bleomycin injury:

Given the importance of cell-cell communications between macrophages and other players, such as alveolar epithelial cells, in the pathogenesis of PF (34), we sought to determine the impact of myeloid-specific miR-33 deficiency on alveolar epithelial cells. Improvement of mitochondrial integrity and function in alveolar type-II cells (AECII) has been shown to have antifibrotic effects (11). We analyzed AECII morphology in the lung tissue of *miR-33*$^{M/M}$*-/-* mice after bleomycin exposure. As previously reported (35), we confirmed that most of the mitochondria in AECIIs of the control mice after bleomycin cells were structurally abnormal and dysmorphic **(Fig. 7A** and **B)**. The morphometric quantification of the mitochondria in AECIIs in the *miR-33*$^{M/M}$*-/-* mice revealed a significant improvement in mitochondrial structure and morphology by area and number at baseline and after bleomycin injury **(Fig. 7A, B,** and **C)**.

After observing that the absence of miR-33 in the macrophages preserves bleomycin-induced mitochondrial abnormalities in AECII, we further aimed to determine the effects of miR-33 ablation on mitochondria-regulated apoptotic pathways. To this end, we performed a TUNEL assay on the lung tissues after bleomycin and identified a significant increase in apoptosis as indicated by TUNEL-positive cells in control mice after bleomycin **(Fig. 7D and E)**. We observed a significant reduction in apoptosis in the lungs of *miR-33*$^{M/M}$*-/-* mice after bleomycin **(Fig. 7D and E)**. We also analyzed whether AECII cells in these mice are protected against apoptosis by combining the TUNEL assay with Pro-SPC IF. We found a significant reduction in apoptosis of AECIIs (double-positive cells) in *miR-33*$^{M/M}$*-/-* mice compared to the control mice after bleomycin exposure (**Fig. 7F** and **G).**

We extended our investigation by performing a deeper analysis of this macrophage-epithelial cell interaction *in vitro*. To this end, we inhibited miR-33 in AM isolated from untreated WT mice and transferred supernatants from these cells after miR-33 ablation to cultured small airway epithelial cells (SAEC). We found that these supernatants significantly reduced bleomycin-induced apoptosis measured by Caspase3/7 activity in SAEC compared to the supernatants from AM treated with scrambled control **(Fig. 7H and I)**, which was concordant with the *in vivo* reduction of the inflammatory cytokines in the BAL of the *miR-33*$^{M/M}$*-/-* mice after bleomycin **(Fig.2H-O)**. This observation provides evidence for beneficial crosstalk from miR-33 depleted macrophages to a key lung structural cell such as AECII.

Our results revealed that the absence of miR-33 in macrophages could have a protective role on AECIIs by improving mitochondrial homeostasis and reducing apoptosis in these cells after bleomycin.

Pharmacological inhibition of miR-33 in lung macrophages protects against ex *vivo* murine models of PF:

To extend our investigation and to confirm the fibro-protective effects of miR-33 ablation using PNA-33 we used murine precision cut lung slices (PCLS) generated from the bleomycin-induced PF model. We isolated lung slices from WT mice on day 14 after bleomycin and treated them with PNA-33 and/or scramble control for 5 days *ex vivo*. We also used PNA-33-TAMRA conjugated to validate the successful uptake of this PNA by macrophages in these PCLS. As shown in **Fig. 8A**, PNA-33 not only accumulates in macrophages in PCLS but also attenuates collagen accumulation measured by second harmonic generation microscopy (SHG) compared to control slices **(Fig. 8A)**. This assay also confirmed there is a significant decrease in fibrogenic gene

expression (*Col1a1* and *Acta2*), as well as an increase in miR-33 target gene expressions (*Pgc-1a*) and (*Abca1*) in PNA-33, treated lung slices compared to controls **(Fig. 8B-D)**.

Pharmacologic inhibition of miR-33 ameliorates fibrosis in human precision cut lung slices from IPF patients:

We sought to assess how the miR-33 inhibition using PNA-33 affects PF in human lungs. We utilized an *ex vivo* culture of human precision cut lung slices (hPCLS) prepared from human IPF lungs and treated with PNA-33 or scramble control for 5 days. At the end of the treatment, we performed bulk RNA sequencing to identify the effects of miR-33 inhibition on gene alterations in these fibrotic lung slices. GVSA analysis did not demonstrate a statistically significant effect on all miR-33 target genes, however, there was a significant increase in the expression of multiple relevant miR-33 target genes including *PPARGC1A* (*PGC-1α*) (P-value=0.03) and ATP Binding Cassette Subfamily G Member1) *ABCG1* (P-value=0.012) after PNA-33 treatment **(Fig. S4A-D).** Further transcriptomic analysis of this IPF PCLS dataset revealed that PNA-33 reduces numerous fibrosis-relevant genes including *ACTA2* (P-Value=0.01, FC=0.7) and multiple collagen genes **(Fig. 8F, Table S3)**.

IPF lung single cell RNA sequencing identified a fibrotic macrophage archetype with a distinct profibrotic signature (6, 36, 37). We evaluated the expression of a signature of 179 profibrotic macrophage genes which are previously reported upregulated in IPF (6, 36, 37), and discovered that PNA-33 treatment significantly reduced the expression of 74 of these genes in IPF PCLS **(Table S4)**. Many of While *CTSK* (Cathepsin K) is the most downregulated gene after miR33 inhibition in IPF PCLS (P-value=0004), the expression of multiple important profibrotic genes from this signature is also decreased including; *CHI3L1* (Chitinase-3-like protein 1) (P-Value=0.003, FC=0.7), *CHIT1* (chitinase 1) (P-Value=0.001, FC=0.8), *ITGA8* (Integrin Subunit

Alpha 8) (P-Value=0.005, FC=0.9), *ITGB5* (Integrin Subunit Beta 5) (P-Value=0.002, FC=0.84), *CCL2* and *CCL4* (C-C Motif Chemokine Ligand) (P-Value=0.01, FC=0.6, and P-Value=0.03, FC=0.54), respectively), *CD36* (cluster of differentiation 36) (P-Value=0.01, FC=0.9) and *MERTK* (MER proto-oncogene, tyrosine kinase) (P-Value=0.01, FC=0.88) **(Fig. 8G, Table S4)**.

To validate PNA-33's ability to attenuate the IPF macrophage disease signature, we also compared the log fold changes of these genes in IPF PCLS following treatment with PNA-33 to the differentially expressed genes in IPF macrophages from ScRNA seq data (from 32 IPF lungs and the 28 controls) (37). Our analysis revealed that miR-33 inhibition attenuated multiple genes from the IPF macrophage's signature list, including, *CHI3L1*, *CHIT1, MERTK, CTSK, ITGB5, FN1*(Fibronectin1), *LGMN* (Legumain), *LPL* (lipoprotein lipase), *FABP5* (Fatty Acid Binding Protein 5), *LIPA* (lipase A) and, *CTSZ* (Cathepsin Z), **(Fig. 8H. Table S5).**

In summary, the analysis of the *ex vivo* lung model of fibrosis demonstrated that miR-33 inhibition has potent antifibrotic effects in human lung tissue at the level of gene expression and alters the profibrotic macrophage gene expression in this setting.

DISCUSSION

Metabolic changes in macrophages are recognized as a key feature in the pathogenesis of chronic lung diseases including PF (38). Here, we demonstrate that these metabolic alterations can be improved in the absence of miR-33. miR-33 regulates key biological and metabolic functions in lung macrophages including bioenergetics, autophagy, mitophagy, and induction of inflammation in response to injury, and the ablation of this miRNA results in improved resolution of fibrosis. Following the observation that levels of miR-33 are substantially increased in BAL cells as well as monocytes isolated from the IPF patients, we studied the role of this miRNA in

296 preclinical models of PF in mice. Genetic deletion of miR-33 in the lung macrophages attenuated
297 PF in the bleomycin mouse model, likely via an improvement in mitochondrial homeostasis, as
298 well as augmentation of autophagy. Pharmacological inhibition of miR-33 using intranasal
299 delivery of PNA-33 in mice model of PF, as well as the 3D culture of murine PCLS and human
300 IPF, established the possibility of a macrophage-specific miR-33 inhibitor as a novel therapeutic
301 approach for PF.

302 The identification of a novel, effective, long-term anti-fibrotic agent that targets the
303 underlying mechanisms of PF is very appealing. Individual miRNAs can modulate the expression
304 of multiple mRNA targets and can have broad effects on multiple cellular pathways. For this
305 reason, therapies targeting individual miRNAs can have a broader impact than traditional single-
306 molecule/single-target approaches. Current anti-miRNA technologies are hindered by
307 physiological and cellular barriers to delivery into target cells. Presenting a targeted lung
308 macrophage miRNA silencing can be a unique and novel therapeutic approach for pulmonary
309 fibrosis. PNAs are synthetic analogs of DNA comprised of nucleobases that are connected to a
310 pseudo-peptide backbone through a carboxymethylene linker (29, 30). The charge-neutral
311 backbone reduces electrostatic repulsion and enables PNAs to hybridize with DNA and bind to
312 single-strand targets with high specificity and affinity. These constructs are also not susceptible to
313 proteases or nucleases, making PNAs ideal molecules for targeting miRNAs[39]. We generated
314 PNA-33 as a specific anti-sense inhibitor of miR-33 and tested the accumulation of this
315 nanoparticle in the lung macrophages after direct delivery to the lung. The strong antifibrotic
316 protection of this system was evident in the animal model of PF as well as the *ex vivo* 3D culture
317 system from mice and human.

There is evidence of the vital role of AMs in the process of PF and they have been presented as the chief effector cells of immune responses with both pro-inflammatory and anti-inflammatory properties (40). miR-33 regulates cellular lipid metabolism and mediates the balance of aerobic glycolysis and mitochondrial oxidative phosphorylation to instruct macrophage inflammatory polarization and shape innate and adaptive immune responses (16, 41, 42). The ability of miR-33 to reprogram immune cells has been identified as a player in the osteoprotective actions of anti-miR-33 therapies (43). Our discovery that the antifibrotic effects of miR-33 ablation are mediated through enhanced mitochondrial homeostasis, as well as augmented autophagy and repression of post-injury inflammation, opens the possibility of a novel pro-mitochondrial anti-miRNA therapy for PF. Furthermore, reprogramming of immune cells via miR-33 inhibition could have important implications for a wide variety of diseases characterized by exaggerated immune responses such as rheumatoid arthritis, and asthma.

There is clear evidence showing the cellular interaction between macrophages and epithelial cells in the process of lung repair and fibrosis (9). It has been shown that during homeostasis, alveolar macrophages interact with alveolar epithelial cells to clear apoptotic cells, environmental particulates, and pathogens (44). Herein we documented that the specific ablation of miR-33 in lung macrophages improves mitochondrial homeostasis in macrophages as well as AECII cells after bleomycin injury. We also demonstrated that these AECII cells are protected against cell death. This striking cell-cell interaction has an important antifibrotic effect, although the cascades of cellular and mechanistic events behind this interaction are yet to be explored.

Autophagy is one of the basic cellular homeostatic processes induced under conditions of stress, and dysregulation of autophagy impacts numerous human diseases including IPF (45). It has been shown that autophagy is not induced in total human IPF lungs and there is a decrease in

the number of autophagosomes observed with electron microscopy in IPF lungs (46). The regulatory role of this important process depends on the cell type and is decreased in lung epithelial cells from IPF patients and in murine models of IPF (47). At the same time, it has been shown that augmenting autophagy in fibroblasts results in the resolution of PF (48). These findings demonstrated that autophagy plays a vital yet complicated role in the pathogenesis of these chronic diseases. In this study, we presented a profound increase in autophagosome formation in miR-33 deficient macrophages after bleomycin injury. It has also been shown that autophagy plays an essential role in the inflammatory response of the lung to infection and stress (49). We demonstrated a significant decrease in the inflammatory response in our model along with this augmentation in autophagy.

Mitophagy is a highly specialized form of autophagy that is induced to clear the dysfunctional mitochondria after the injury. Insufficient mitophagy gives rise to the accumulation of damaged mitochondria and it is implicated in a cell-specific manner in the pathogenesis of IPF (35, 50, 51). Mitochondrial quality control in lung macrophages is a critical determinant of PF. Diminished mitochondrial quality control results in augmented mitochondrial dysfunction and increased mtROS that leads to PF by promoting profibrotic macrophages (52). The absence of miR-33 in the macrophages leads to an augmentation of autophagy as well as mitophagy, which results in the resolution of fibrosis by polarizing the macrophages from profibrotic to anti-fibrotic.

Macrophages are innate immune cells and the interplay between pro-inflammatory/anti-inflammatory macrophage phenotypes has been suggested to play a key role in the development and progression of lung fibrosis as well as inhibit fibrosis (53-55). The recent findings from single cell RNA sequencing data from mice and human lung fibrosis revealed the presence of a distinct profibrotic macrophage subtype in the fibrotic lung with a higher level of *CHI3L1*. *CHIT1*, *APOE,*

and Integrins (36, 37, 56-58). Inhibiting miR-33 in PCLS isolated from IPF patients not only decreased the expression of *ACTA2* and Collagen but also altered the expression of genes known to be expressed in profibrotic macrophages, suggesting an effect on this population.

AMPK is a critical cell bioenergetic sensor and metabolic regulator (56). Importantly, previous studies have demonstrated that AMPK activators such as metformin exert protective effects on lung injury (48). In addition to AMPK, PGC-1α is another master regulator of metabolic reprogramming and inducer of mitochondrial biogenesis, and we previously discovered that thyroid hormone (T3) inhibits lung fibrosis by restoring mitochondrial health and function through a PGC-1α-dependent pathway (11, 13). miR-33 has previously been shown to regulate mitochondrial homeostasis by targeting both *Pgc-1α* and *Ampk* in the context of atherosclerosis (17, 22, 59). The importance of the AMPK-SIRT3-PGC-1α pathway in the regulation of metabolic remodeling is also well-known (60, 61). AMPK and PGC-1α may modulate autophagy, apoptosis, inflammation, and mitochondrial function through SIRT3 signaling (62, 63). In this work, we confirmed a significant increase in the expression levels of AMPK, PGC-1α, and SIRT3 in miR-33 deficient macrophages, which their downstream effects might be responsible for the resolution of PF via an increase in autophagy, decrease in apoptosis, amelioration of the inflammation and improvement of mitochondrial homeostasis.

Despite elucidating the role of miR-33 in regulating macrophage immune-metabolic response during lung fibrosis, we did not address several important mechanistic insights in this study. For Instance, we did not explore the role of lipid metabolism and FAO in the pathogenesis of lung fibrosis. The contribution of miR-33 in regulating lipid metabolism is well established (18-23, 26, 42, 64), although the relationship between this concept and lung fibrosis still needs to be explored. In the current study, while we provide strong experimental evidence suggesting active

crosstalk between macrophages and other cells in the lung such as epithelial cells, the molecular mechanism that mediates these profibrotic responses need to be further elucidated. Finally, many of our analyses were based on the comparison between advanced IPF samples with disease-free controls; miR-33 may have different effects in different stages of the progression of IPF, or in other advanced lung diseases, thus, future studies will need to assess Mir-33 and its targets in different stages of IPF and other lung diseases.

Herein using *in vivo* and ex *vivo* models of PF, we demonstrated that genetic and pharmacologic inhibition of miR-33 in macrophages attenuates lung fibrosis via improvement of mitochondrial homeostasis and augmentation of autophagy. Finally, we propose an efficient targeted therapy for PF that could be further evaluated as a therapeutic strategy in humans.

MATERIALS AND METHODS

In vitro Experiments.

Primary mouse alveolar macrophages (AM) isolation.

AM was isolated as previously described (65). Briefly, bronchoalveolar lavage was harvested by slowly injecting and withdrawing 1 ml of PBS into the lung three times through a cannula in the trachea. BAL fluid was centrifuged (300 ×g, 5min), the cell pellet was washed in PBS, and cells were plated and used for different purposes as described in the appropriate figure legend. For miR-33 inhibition in initial *in vitro* studies miR-33 antagomir was purchased from Dharmacon and transfected using lipofectamine RNAiMAX (ThermofiserScinetific) according to the manufacturer's protocols.

Cell isolation from human lungs.

Human immune cells were isolated from fresh human lung samples as previously described (66, 67). Briefly, 2-3 grams of tissue were used for digestion using (1 mg/mL Collagenase/Dispase (Roche), 3 U/mL Elastase (Worthington), and 20 U/ mL DNAse (Roche) for 30 min at 37 degrees. All CD-45 positive and negative cells were isolated using MACS (Miltenyi Biotec Inc.) according to the manufacturer's protocol.

***In vivo* Experiments.**

Generation of macrophage-specific miR-33 deficient mice.

Generation of conditional miR-33 knockout mice *(miR-33$^{loxP/loxP}$)* was accomplished with the assistance of Cyagen Biosciences Inc. The success of this approach has been verified by Southern blotting and confirmed by PCR-based genotyping using specific primers. To generate macrophage/monocyte specific miR-33 Deficient mice, *miR-33$^{loxP/loxP}$* mice were crossed with *LysM^{Cre}* mice from Jackson Laboratories (004781).

Bleomycin-induced mice model of pulmonary Fibrosis.

miR-33 macrophage-specific knockout (KO) mice (*miR-33$^{M/M}$-/-),* and appropriate controls (*miR-33$^{M/M}$*+/+) *were used* in a bleomycin-induced PF model. Briefly, PF was induced in mice by intrapulmonary delivery of bleomycin (1.5 U/kg) or 0.9% normal saline via oropharyngeal instillation. Mice were euthanized, and lungs were harvested on day 14 for fibrosis analysis. Mice were randomly assigned to groups. Mice of both sexes were studied and 10-15 mice per group were used. The bleomycin challenge was not blinded, but the analysis of animal samples was. All animal model experiments were performed three times.

Pharmacological inhibition of miR-33 in mice.

All mice used for this study were WT C57/BL6 (Jackson Laboratories). PF was induced in mice by intrapulmonary delivery of bleomycin (1.5 U/kg) or 0.9% normal saline via oropharyngeal instillation. PNA-33 or scramble control was administered intranasally (2mg/kg) on day 7 after the bleomycin injury and repeated every 3 days. Mice were euthanized, and lungs were harvested on day 21 for fibrosis analysis.

***Ex vivo* Experiments.**

Precision cut lung slices.

Mouse precision cut lung slices (mPCLS): were generated as previously described (68-70). Mouse lungs from both vehicle and bleomycin (day 14) models were used and repeated accordingly. Briefly, low melting grade agarose (3 wt-%) was slowly injected via the trachea to artificially inflate the lung. Lungs were cooled at 4°C for 15 minutes to allow gelling of the agarose and then cut to a thickness of 150µm using a Compresstome (VF-300-0Z by Precisionary®) at a cutting speed of 6 µm/s and the oscillation frequency of 5Hz. The mPCLS were cultured in 24 multi-well plates (Corning®) in 500µL DMEM-F12 no-phenol red containing 0.1% FBS and 1% penicillin/streptomycin 37 °C, 5% CO_2, and 95% humidity. Treatment with PNA-33 or scramble control was administered in the first 24 hours after slicing, all media were changed daily, and lung slices were isolated 5 days after treatment for analysis. Serial live imaging of lung slices by second harmonic generation microscopy technique was performed before (Time; 0 hours) and after each treatment (Time;120 hours) (71). mPCLS were fixed with 4% (weight/volume) paraformaldehyde overnight, and paraffin was embedded at 0h and 120h. 3µm sections were cut using a microtome, mounted on glass slides, and subjected to antigen retrieval. After deparaffinization and rehydration, staining was performed according to standard protocols for Masson's trichrome.

Finally, samples were mounted using a mounting medium and covered with a cover slip. Microscopic scanning of the slides was conducted in bright field (BF) with a Nikon inverted microscope at 20X magnification. 2 representative images were acquired for each sample and at least 20 different random fields of view were used for collagen quantification. RNA was isolated from 5-6 replicated lung slices from each treatment using miRNeasy mini kit (Qiagen) at time 0 and time 120 hours for all groups. mRNA levels of fibrogenic genes were quantified by TaqMan qPCR and normalized to GAPDH expression. All experimental groups were performed in a group of 6 technical replicates and repeated at least three times.

Human precision cut lung slices (hPCLS): Cryopreserved 300µm thick sections of human lungs, derived from the patients with IPF were cultured and treated with, and used for this study. Briefly, the right middle and lung lower lobes are inflated by injecting 2% warm (37°C) low-melting agarose, and peripheral slices (300 µm thick) are cut with a vibratome and then punched to a diameter of 4 mm using a biopsy punch (69). Individual PCLS/punches were treated with PNA-33 or scramble control for 5 days. All IPF PCLS were harvested at the end of the 5 days treatment and used RNA extraction using miRNeasy mini kit (Qiagen) for further analysis.

RNA sequencing.

Total RNA from all IPF PCLS samples was extracted with miRNeasy Mini Kit (Qiagen-217004) according to the manufacturer's instructions. The purity of the RNA was verified using a NanoDrop at 260 nm, and the quality of the RNA was assessed using the Agilent 2100 Bioanalyzer (Agilent Technologies). Libraries were prepared using KAPA Stranded mRNA-Seq Kit. mRNA was enriched by ribosomal RNA depletion. Library quality was checked using an Agilent TapeStation analyzer and sequencing was performed with NovaSeq (2X100, 25 M reads per

sample). FastQC files were generated and trimmed (https://www.bioinformatics.babraham.ac.uk/projects/trim_galore/) and a quality review was performed by FastQC (http://www.bioinformatics.babraham.ac.uk/projects/fastqc/) before and after quality trim. Reads were aligned with STAR aligner (version 2.6.1d, using the default settings) to the HG38 human genome and ENSEMBL94 annotation GTF file. After alignment and summarization with featureCounts of the Subread package (feature Counts release 1.6.3 and Picard version 2.18.21), data was normalized and differential expression was carried out with edgR package[72] and implemented in R.

For comparing the effect of miR-33 inhibition in IPF PCLS to IPF lung macrophage signature, processed scRNAseq data of IPF and control lungs (37) was downloaded from GEO accession GSE136831. Gene expression counts were normalized by scaling values to 10,000 transcripts per cell, then natural log transformation with a pseudo count of 1. IPF and control cells labeled as "Macrophage" (37) were extracted from the entire dataset, and average normalized gene expression values of all genes were calculated for each subject (32 IPF; 28 controls); these average per subject values were then used for a student's t-test comparing IPF and control values; the resulting p-values were adjusted for false discovery rate (FDR). Non-ribosomal genes with an adjusted p-value below 0.5 and absolute log fold change greater than 0.07 were used to represent differentially expressed genes in IPF macrophage; of these 1,197 genes, 1,181 genes were also evaluated via bulk RNAseq of IPF PCLS either treated or untreated with miR-33 inhibitor. To evaluate mir-33 inhibition's ability to attenuate the IPF macrophage disease signature, we compare the log fold changes of these genes in *ex vivo* IPF PCLS following treatment with miR-33 inhibitor to the reported log fold changes in IPF versus control lung macrophage *in vivo*.

Detailed methods are provided in the online data supplement.

\

Statistical analyses.

For *in vitro* and *in vivo* assays statistical analysis was performed by GraphPad Prism version 8.1.2. Results were analyzed by Mann–Whitney *U* test for comparisons of two groups when sample data were not normally distributed, by unpaired Student's -*t*-test for comparisons of two groups with normal distribution, and by one-way ANOVA with Student–Newman–Keuls *post hoc* test for pairwise comparisons of three or more groups or more than 10 per group and by Kruskal-Wallis one way analysis of variance for comparison of groups with fewer than 10 samples per group followed by Dunn's post hoc test for pairwise comparisons. Efficacy experiments were designed for ten-fifteen animals in the control and treated groups, to allow for 82% power to detect a difference of 20% between the two groups at a statistical significance level of 0.05, but the actual size of the groups differed because of mortality. All data were presented as (means+ SEM) and the differences were considered statistically significant at $P < 0.05$. Unless specified in the text, data are expressed as means of at least 3 independent experiments. Fold change for qPCR was determined using the 2^-ΔΔCt method (Livak).

Studies approval.

Human studies. Demographic characteristics of the BAL Freiburg cohort (73) used for miR-33 measurements are described in **Table S1**. IPF diagnosis was established by a multidisciplinary board according to the American Thoracic Society/European Respiratory Society criteria and was later determined to be consistent with recent guidelines (74). Healthy age and sex-matched controls were used from the healthy volunteers and the lung disease was ruled

525 out by pulmonary function test and clinical examination (73). Demographic characteristics of the
526 IPF explant lung samples used for cell isolation used are described in **Table S2**. Age and sex-
527 matched healthy lungs were from rejected donor lung organs that underwent lung transplantation
528 at the Brigham and Women's Hospital, or donor organs provided by the National Disease Research
529 Interchange (NDRI). The study protocol was approved by the Partners Healthcare Institutional
530 Board Review (IRB Protocol ID: 2011P002419) and the Yale University Institutional Review
531 Board (IRB Protocol ID: 2000022618).

532 **Animal studies.** -All mice were housed and used for the experiments under the direction
533 and approved protocols. All animal studies were conducted in accordance with the NIH guidelines
534 for the humane treatment of animals and were approved by the Institutional Animal Care and Use
535 Committee (IACUC), of Yale University.

536

537 **ACKNOWLEDGMENTS.**

538 We would like to express our gratitude to the Electron Microscopy facility at the Center
539 for Cellular and Molecular Imaging (CCMI) as well as *in vivo* imaging facility at Yale School of
540 Medicine for all the help they provided for tissue processing and imaging for this study. **Author**
541 **contributions.** F.A., C.F.H., and N.K. conceptualized, acquired funding, and supervised the study.
542 N.L.P and C.F.H. generated macrophage-specific miR-33 knockout (KO) and provided the
543 necessary guidance for this project. All experiments in this study were performed by F.A., N.L.P.,
544 S.M., M.C., J.K., S.P.P., T.B., S.D., C.C.J, K.S.R., J.E.M., N.R.A., G.I., N.O., J.C.S., G.D., and
545 T.A. PNA-33 was designed and generated by S.M. and R.B. L.K.S., C.R., C.S.D. provided
546 guidance and necessary supports for this project. A.P., J.V.N., and I.R. provided BAL and human
547 lung tissues from IPF and controls for this study. The manuscript was drafted by F.A., N.L.P.,

R.B., C.F.H., and N.K. and was reviewed and edited by all other authors**. Funding.** This work was supported by grants from the National Institutes of Health (NIH R01HL141852, R01HL127349, U01HL145567, and U01HL122626 to N.K. and R35HL135820 to C.F.H.) and BI Discovery Award 19-004578 to F.A. **Competing interests.** NK served as a consultant to Biogen Idec, Boehringer Ingelheim, Third Rock, Pliant, Samumed, NuMedii, Theravance, LifeMax, Three Lake Partners, Optikira, Astra Zeneca, RohBar, Veracyte, Augmanity, CSL Behring, Galapagos and Thyron over the last 3 years, reports Equity in Pliant and Thyron, and grants from Veracyte, Boehringer Ingelheim, BMS and non-financial support from MiRagen and Astra Zeneca. NK has IP on novel biomarkers and therapeutics in IPF licensed to Biotech. C.F.H. has a patent on the use of miR-33 inhibitors to treat inflammation. **Data and materials availability:** All data, code, and materials used in the analysis is available to any researcher for purposes of reproducing or extending the analysis. All raw count expression data from *ex vivo* studies were deposited to the Gene Expression Omnibus (GEO) and the accession number is GSE215948.

REFERENCES

1. Meyer KC. Pulmonary fibrosis, part I: epidemiology, pathogenesis, and diagnosis. *Expert Rev Respir Med.* 2017;11(5):343-59.
2. Maher TM, Bendstrup E, Dron L, Langley J, Smith G, Khalid JM, Patel H, and Kreuter M. Global incidence and prevalence of idiopathic pulmonary fibrosis. *Respir Res.* 2021;22(1):197.
3. Wijsenbeek M, Kreuter M, Olson A, Fischer A, Bendstrup E, Wells CD, Denton CP, Mounir B, Zouad-Lejour L, Quaresma M, et al. Progressive fibrosing interstitial lung

diseases: current practice in diagnosis and management. *Curr Med Res Opin.* 2019;35(11):2015-24.

4. Lederer DJ, and Martinez FJ. Idiopathic Pulmonary Fibrosis. *N Engl J Med.* 2018;379(8):797-8.

5. Wynn TA, and Vannella KM. Macrophages in Tissue Repair, Regeneration, and Fibrosis. *Immunity.* 2016;44(3):450-62.

6. Morse C, Tabib T, Sembrat J, Buschur KL, Bittar HT, Valenzi E, Jiang Y, Kass DJ, Gibson K, Chen W, et al. Proliferating SPP1/MERTK-expressing macrophages in idiopathic pulmonary fibrosis. *Eur Respir J.* 2019;54(2).

7. Reyfman PA, Walter JM, Joshi N, Anekalla KR, McQuattie-Pimentel AC, Chiu S, Fernandez R, Akbarpour M, Chen CI, Ren Z, et al. Single-Cell Transcriptomic Analysis of Human Lung Provides Insights into the Pathobiology of Pulmonary Fibrosis. *Am J Respir Crit Care Med.* 2018.

8. Warheit-Niemi HI, Hult EM, and Moore BB. A pathologic two-way street: how innate immunity impacts lung fibrosis and fibrosis impacts lung immunity. *Clin Transl Immunology.* 2019;8(6):e1065.

9. Cheng P, Li S, and Chen H. Macrophages in Lung Injury, Repair, and Fibrosis. *Cells.* 2021;10(2).

10. Ishikawa G, Liu A, and Herzog EL. Evolving Perspectives on Innate Immune Mechanisms of IPF. *Front Mol Biosci.* 2021;8(676569.

11. Yu G, Tzouvelekis A, Wang R, Herazo-Maya JD, Ibarra GH, Srivastava A, de Castro JPW, DeIuliis G, Ahangari F, Woolard T, et al. Thyroid hormone inhibits lung fibrosis in mice by improving epithelial mitochondrial function. *Nat Med.* 2018;24(1):39-49.

12. Bueno M, Calyeca J, Rojas M, and Mora AL. Mitochondria dysfunction and metabolic reprogramming as drivers of idiopathic pulmonary fibrosis. *Redox Biology.* 2020;33(101509.

13. Zank DC, Bueno M, Mora AL, and Rojas M. Idiopathic Pulmonary Fibrosis: Aging, Mitochondrial Dysfunction, and Cellular Bioenergetics. *Front Med (Lausanne).* 2018;5(10.

14. Tsitoura E, Vasarmidi E, Bibaki E, Trachalaki A, Koutoulaki C, Papastratigakis G, Papadogiorgaki S, Chalepakis G, Tzanakis N, and Antoniou KM. Accumulation of damaged mitochondria in alveolar macrophages with reduced OXPHOS related gene expression in IPF. *Respir Res.* 2019;20(1):264.

15. Henderson NC, Rieder F, and Wynn TA. Fibrosis: from mechanisms to medicines. *Nature.* 2020;587(7835):555-66.

16. Ouimet M, Ediriweera HN, Gundra UM, Sheedy FJ, Ramkhelawon B, Hutchison SB, Rinehold K, van Solingen C, Fullerton MD, Cecchini K, et al. MicroRNA-33-dependent regulation of macrophage metabolism directs immune cell polarization in atherosclerosis. *J Clin Invest.* 2015;125(12):4334-48.

17. Price NL, and Fernandez-Hernando C. Novel Role of miR-33 in Regulating of Mitochondrial Function. *Circ Res.* 2015;117(3):225-8.

18. Rayner KJ, Suarez Y, Davalos A, Parathath S, Fitzgerald ML, Tamehiro N, Fisher EA, Moore KJ, and Fernandez-Hernando C. MiR-33 contributes to the regulation of cholesterol homeostasis. *Science.* 2010;328(5985):1570-3.

19. Rayner KJ, Esau CC, Hussain FN, McDaniel AL, Marshall SM, van Gils JM, Ray TD, Sheedy FJ, Goedeke L, Liu X, et al. Inhibition of miR-33a/b in non-human primates raises plasma HDL and lowers VLDL triglycerides. *Nature.* 2011;478(7369):404-7.

20. Horie T, Ono K, Horiguchi M, Nishi H, Nakamura T, Nagao K, Kinoshita M, Kuwabara Y, Marusawa H, Iwanaga Y, et al. MicroRNA-33 encoded by an intron of sterol regulatory element-binding protein 2 (Srebp2) regulates HDL in vivo. *Proc Natl Acad Sci U S A.* 2010;107(40):17321-6.

21. Marquart TJ, Allen RM, Ory DS, and Baldan A. miR-33 links SREBP-2 induction to repression of sterol transporters. *Proc Natl Acad Sci U S A.* 2010;107(27):12228-32.

22. Davalos A, Goedeke L, Smibert P, Ramirez CM, Warrier NP, Andreo U, Cirera-Salinas D, Rayner K, Suresh U, Pastor-Pareja JC, et al. miR-33a/b contribute to the regulation of fatty acid metabolism and insulin signaling. *Proc Natl Acad Sci U S A.* 2011;108(22):9232-7.

23. Najafi-Shoushtari SH, Kristo F, Li Y, Shioda T, Cohen DE, Gerszten RE, and Naar AM. MicroRNA-33 and the SREBP host genes cooperate to control cholesterol homeostasis. *Science.* 2010;328(5985):1566-9.

24. Karunakaran D, Thrush AB, Nguyen MA, Richards L, Geoffrion M, Singaravelu R, Ramphos E, Shangari P, Ouimet M, Pezacki JP, et al. Macrophage Mitochondrial Energy Status Regulates Cholesterol Efflux and Is Enhanced by Anti-miR33 in Atherosclerosis. *Circ Res.* 2015;117(3):266-78.

25. Zhang X, and Fernandez-Hernando C. miR-33 Regulation of Adaptive Fibrotic Response in Cardiac Remodeling. *Circ Res.* 2017;120(5):753-5.

26. Price NL, Miguel V, Ding W, Singh AK, Malik S, Rotllan N, Moshnikova A, Toczek J, Zeiss C, Sadeghi MM, et al. Genetic deficiency or pharmacological inhibition of miR-33 protects from kidney fibrosis. *JCI Insight.* 2019;4(22).

27. Price NL, Zhang X, Fernandez-Tussy P, Singh AK, Burnap SA, Rotllan N, Goedeke L, Sun J, Canfran-Duque A, Aryal B, et al. Loss of hepatic miR-33 improves metabolic homeostasis and liver function without altering body weight or atherosclerosis. *Proc Natl Acad Sci U S A.* 2021;118(5).

28. Sato T, Baskoro H, Rennard SI, Seyama K, and Takahashi K. MicroRNAs as Therapeutic Targets in Lung Disease: Prospects and Challenges. *Chronic Obstr Pulm Dis.* 2015;3(1):382-8.

29. Egholm M, Buchardt O, Christensen L, Behrens C, Freier SM, Driver DA, Berg RH, Kim SK, Norden B, and Nielsen PE. PNA hybridizes to complementary oligonucleotides obeying the Watson-Crick hydrogen-bonding rules. *Nature (London).* 1993;365(6446):566-8.

30. Nielsen PE, Egholm M, Berg RH, and Buchardt O. Sequence-selective recognition of DNA by strand displacement with a thymine-substituted polyamide. *Science (Washington, D C, 1883-).* 1991;254(5037):1497-500.

31. Cheng CJ, Bahal R, Babar IA, Pincus Z, Barrera F, Liu C, Svoronos A, Braddock DT, Glazer PM, Engelman DM, et al. MicroRNA silencing for cancer therapy targeted to the tumour microenvironment. *Nature.* 2015;518(7537):107-10.

32. Ryu C, Sun H, Gulati M, Herazo-Maya JD, Chen Y, Osafo-Addo A, Brandsdorfer C, Winkler J, Blaul C, Faunce J, et al. Extracellular Mitochondrial DNA Is Generated by

Fibroblasts and Predicts Death in Idiopathic Pulmonary Fibrosis. *Am J Respir Crit Care Med.* 2017;196(12):1571-81.

33. Ashrafi G, and Schwarz TL. The pathways of mitophagy for quality control and clearance of mitochondria. *Cell Death Differ.* 2013;20(1):31-42.

34. Bhattacharya J, and Westphalen K. Macrophage-epithelial interactions in pulmonary alveoli. *Semin Immunopathol.* 2016;38(4):461-9.

35. Bueno M, Lai YC, Romero Y, Brands J, St Croix CM, Kamga C, Corey C, Herazo-Maya JD, Sembrat J, Lee JS, et al. PINK1 deficiency impairs mitochondrial homeostasis and promotes lung fibrosis. *J Clin Invest.* 2015;125(2):521-38.

36. Reyfman PA, Walter JM, Joshi N, Anekalla KR, McQuattie-Pimentel AC, Chiu S, Fernandez R, Akbarpour M, Chen CI, Ren Z, et al. Single-Cell Transcriptomic Analysis of Human Lung Provides Insights into the Pathobiology of Pulmonary Fibrosis. *Am J Respir Crit Care Med.* 2019;199(12):1517-36.

37. Adams TS, Schupp JC, Poli S, Ayaub EA, Neumark N, Ahangari F, Chu SG, Raby BA, DeIuliis G, Januszyk M, et al. Single-cell RNA-seq reveals ectopic and aberrant lung-resident cell populations in idiopathic pulmonary fibrosis. *Sci Adv.* 2020;6(28):eaba1983.

38. Ogger PP, and Byrne AJ. Macrophage metabolic reprogramming during chronic lung disease. *Mucosal Immunol.* 2021;14(2):282-95.

39. Demidov VV, Potaman VN, Frank-Kamenetskii MD, Egholm M, Buchard O, Sonnichsen SH, and Nielsen PE. Stability of peptide nucleic acids in human serum and cellular extracts. *Biochem Pharmacol.* 1994;48(6):1310-3.

40. Zhang L, Wang Y, Wu G, Xiong W, Gu W, and Wang CY. Macrophages: friend or foe in idiopathic pulmonary fibrosis? *Respir Res.* 2018;19(1):170.

680 41. Price NL, Rotllan N, Canfran-Duque A, Zhang X, Pati P, Arias N, Moen J, Mayr M, Ford
681 DA, Baldan A, et al. Genetic Dissection of the Impact of miR-33a and miR-33b during the
682 Progression of Atherosclerosis. *Cell Rep.* 2017;21(5):1317-30.
683 42. Price NL, Goedeke L, Suarez Y, and Fernandez-Hernando C. miR-33 in cardiometabolic
684 diseases: lessons learned from novel animal models and approaches. *EMBO Mol Med.*
685 2021;13(5):e12606.
686 43. Afonso MS, Sharma M, Schlegel M, van Solingen C, Koelwyn GJ, Shanley LC, Beckett
687 L, Peled D, Rahman K, Giannarelli C, et al. miR-33 Silencing Reprograms the Immune
688 Cell Landscape in Atherosclerotic Plaques. *Circ Res.* 2021;128(8):1122-38.
689 44. Young LR, Gulleman PM, Short CW, Tanjore H, Sherrill T, Qi A, McBride AP,
690 Zaynagetdinov R, Benjamin JT, Lawson WE, et al. Epithelial-macrophage interactions
691 determine pulmonary fibrosis susceptibility in Hermansky-Pudlak syndrome. *JCI Insight.*
692 2016;1(17):e88947.
693 45. Patel AS, Lin L, Geyer A, Haspel JA, An CH, Cao J, Rosas IO, and Morse D. Autophagy
694 in idiopathic pulmonary fibrosis. *PLoS One.* 2012;7(7):e41394.
695 46. Margaritopoulos GA, Tsitoura E, Tzanakis N, Spandidos DA, Siafakas NM, Sourvinos G,
696 and Antoniou KM. Self-eating: friend or foe? The emerging role of autophagy in idiopathic
697 pulmonary fibrosis. *Biomed Res Int.* 2013;2013(420497.
698 47. Zhao H, Wang Y, Qiu T, Liu W, and Yao P. Autophagy, an important therapeutic target
699 for pulmonary fibrosis diseases. *Clin Chim Acta.* 2020;502(139-47.
700 48. Rangarajan S, Bone NB, Zmijewska AA, Jiang S, Park DW, Bernard K, Locy ML, Ravi S,
701 Deshane J, Mannon RB, et al. Metformin reverses established lung fibrosis in a bleomycin
702 model. *Nat Med.* 2018;24(8):1121-7.

703 49. Racanelli AC, Kikkers SA, Choi AMK, and Cloonan SM. Autophagy and inflammation in
704 chronic respiratory disease. *Autophagy.* 2018;14(2):221-32.
705 50. Kobayashi K, Araya J, Minagawa S, Hara H, Saito N, Kadota T, Sato N, Yoshida M,
706 Tsubouchi K, Kurita Y, et al. Involvement of PARK2-Mediated Mitophagy in Idiopathic
707 Pulmonary Fibrosis Pathogenesis. *J Immunol.* 2016;197(2):504-16.
708 51. Aggarwal S, Mannam P, and Zhang J. Differential regulation of autophagy and mitophagy
709 in pulmonary diseases. *Am J Physiol Lung Cell Mol Physiol.* 2016;311(2):L433-52.
710 52. Larson-Casey JL, He C, and Carter AB. Mitochondrial quality control in pulmonary
711 fibrosis. *Redox Biol.* 2020;33(101426.
712 53. Goda C, Balli D, Black M, Milewski D, Le T, Ustiyan V, Ren X, Kalinichenko VV, and
713 Kalin TV. Loss of FOXM1 in macrophages promotes pulmonary fibrosis by activating p38
714 MAPK signaling pathway. *PLoS Genet.* 2020;16(4):e1008692.
715 54. Liu G, Zhai H, Zhang T, Li S, Li N, Chen J, Gu M, Qin Z, and Liu X. New therapeutic
716 strategies for IPF: Based on the "phagocytosis-secretion-immunization" network
717 regulation mechanism of pulmonary macrophages. *Biomed Pharmacother.*
718 2019;118(109230.
719 55. Desai O, Winkler J, Minasyan M, and Herzog EL. The Role of Immune and Inflammatory
720 Cells in Idiopathic Pulmonary Fibrosis. *Front Med (Lausanne).* 2018;5(43.
721 56. Schupp JC, Khanal S, Gomez JL, Sauler M, Adams TS, Chupp GL, Yan X, Poli S, Zhao
722 Y, Montgomery RR, et al. Single-Cell Transcriptional Archetypes of Airway Inflammation
723 in Cystic Fibrosis. *Am J Respir Crit Care Med.* 2020;202(10):1419-29.
724 57. Misharin AV, Morales-Nebreda L, Reyfman PA, Cuda CM, Walter JM, McQuattie-
725 Pimentel AC, Chen CI, Anekalla KR, Joshi N, Williams KJN, et al. Monocyte-derived

alveolar macrophages drive lung fibrosis and persist in the lung over the life span. *The Journal of experimental medicine.* 2017;214(8):2387-404.

58. Habermann AC, Gutierrez AJ, Bui LT, Yahn SL, Winters NI, Calvi CL, Peter L, Chung MI, Taylor CJ, Jetter C, et al. Single-cell RNA sequencing reveals profibrotic roles of distinct epithelial and mesenchymal lineages in pulmonary fibrosis. *Sci Adv.* 2020;6(28):eaba1972.

59. Karunakaran D, Richards L, Geoffrion M, Barrette D, Gotfrit RJ, Harper ME, and Rayner KJ. Therapeutic Inhibition of miR-33 Promotes Fatty Acid Oxidation but Does Not Ameliorate Metabolic Dysfunction in Diet-Induced Obesity. *Arterioscler Thromb Vasc Biol.* 2015;35(12):2536-43.

60. Xu M, Xue RQ, Lu Y, Yong SY, Wu Q, Cui YL, Zuo XT, Yu XJ, Zhao M, and Zang WJ. Choline ameliorates cardiac hypertrophy by regulating metabolic remodelling and UPRmt through SIRT3-AMPK pathway. *Cardiovasc Res.* 2019;115(3):530-45.

61. Zhang T, Liu J, Shen S, Tong Q, Ma X, and Lin L. SIRT3 promotes lipophagy and chaperon-mediated autophagy to protect hepatocytes against lipotoxicity. *Cell Death Differ.* 2020;27(1):329-44.

62. Maissan P, Mooij EJ, and Barberis M. Sirtuins-Mediated System-Level Regulation of Mammalian Tissues at the Interface between Metabolism and Cell Cycle: A Systematic Review. *Biology (Basel).* 2021;10(3).

63. Zhang T, Fang Z, Linghu KG, Liu J, Gan L, and Lin L. Small molecule-driven SIRT3-autophagy-mediated NLRP3 inflammasome inhibition ameliorates inflammatory crosstalk between macrophages and adipocytes. *Br J Pharmacol.* 2020;177(20):4645-65.

64. Price NL, Singh AK, Rotllan N, Goedeke L, Wing A, Canfran-Duque A, Diaz-Ruiz A, Araldi E, Baldan A, Camporez JP, et al. Genetic Ablation of miR-33 Increases Food Intake, Enhances Adipose Tissue Expansion, and Promotes Obesity and Insulin Resistance. *Cell Rep.* 2018;22(8):2133-45.

65. Zhang X, Goncalves R, and Mosser DM. The isolation and characterization of murine macrophages. *Curr Protoc Immunol.* 2008;Chapter 14(Unit 14 1.

66. Yu YA, and Tighe RM. Isolation and Characterization of Human Lung Myeloid Cells. *Methods Mol Biol.* 2018;1809(111-9.

67. Bantikassegn A, Song X, and Politi K. Isolation of epithelial, endothelial, and immune cells from lungs of transgenic mice with oncogene-induced lung adenocarcinomas. *Am J Respir Cell Mol Biol.* 2015;52(4):409-17.

68. Lehmann M, Buhl L, Alsafadi HN, Klee S, Hermann S, Mutze K, Ota C, Lindner M, Behr J, Hilgendorff A, et al. Differential effects of Nintedanib and Pirfenidone on lung alveolar epithelial cell function in ex vivo murine and human lung tissue cultures of pulmonary fibrosis. *Respir Res.* 2018;19(1):175.

69. Alsafadi HN, Staab-Weijnitz CA, Lehmann M, Lindner M, Peschel B, Konigshoff M, and Wagner DE. An ex vivo model to induce early fibrosis-like changes in human precision-cut lung slices. *Am J Physiol Lung Cell Mol Physiol.* 2017;312(6):L896-L902.

70. Uhl FE, Vierkotten S, Wagner DE, Burgstaller G, Costa R, Koch I, Lindner M, Meiners S, Eickelberg O, and Konigshoff M. Preclinical validation and imaging of Wnt-induced repair in human 3D lung tissue cultures. *Eur Respir J.* 2015;46(4):1150-66.

71. Liu Y, Keikhosravi A, Mehta GS, Drifka CR, and Eliceiri KW. Methods for Quantifying Fibrillar Collagen Alignment. *Methods Mol Biol.* 2017;1627(429-51.

72. Robinson MD, McCarthy DJ, and Smyth GK. edgeR: a Bioconductor package for differential expression analysis of digital gene expression data. *Bioinformatics.* 2010;26(1):139-40.

73. Prasse A, Binder H, Schupp JC, Kayser G, Bargagli E, Jaeger B, Hess M, Rittinghausen S, Vuga L, Lynn H, et al. BAL Cell Gene Expression Is Indicative of Outcome and Airway Basal Cell Involvement in Idiopathic Pulmonary Fibrosis. *Am J Respir Crit Care Med.* 2019;199(5):622-30.

74. Raghu G, Collard HR, Egan JJ, Martinez FJ, Behr J, Brown KK, Colby TV, Cordier JF, Flaherty KR, Lasky JA, et al. An official ATS/ERS/JRS/ALAT statement: idiopathic pulmonary fibrosis: evidence-based guidelines for diagnosis and management. *Am J Respir Crit Care Med.* 2011;183(6):788-824.

Figures.

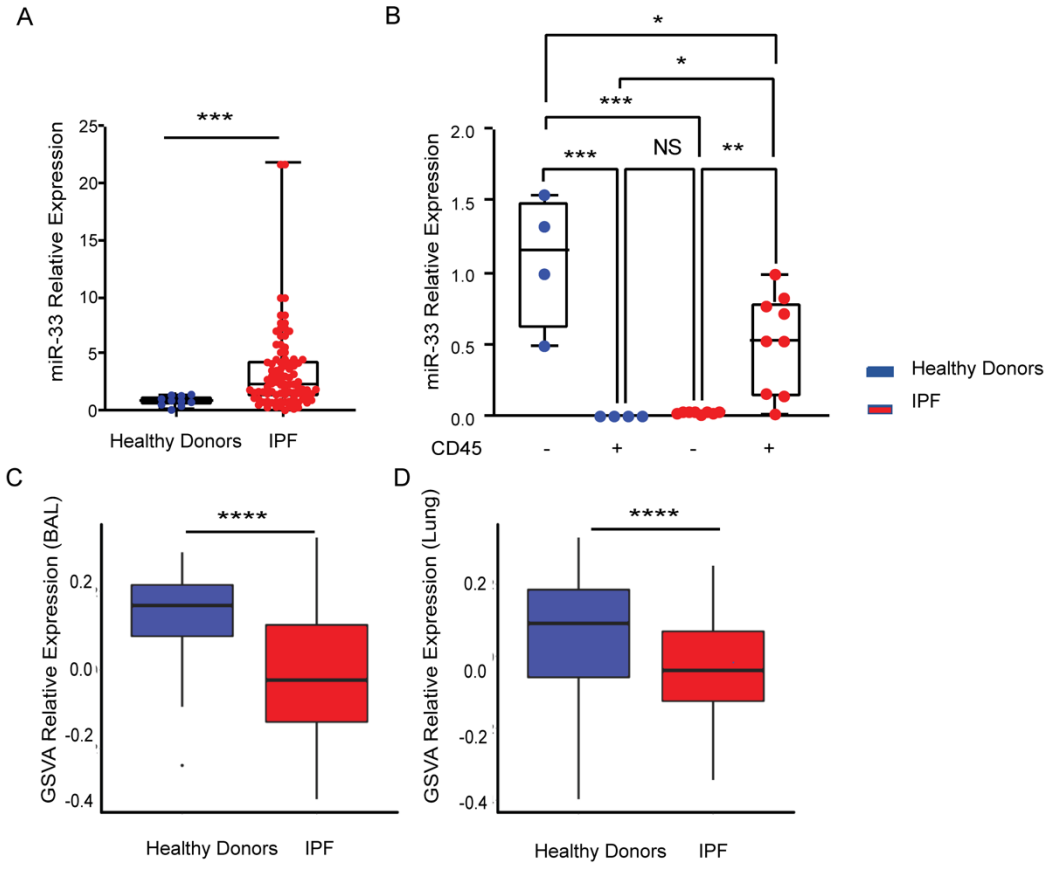

Figure 1. miR-33 levels increase in BAL and lung CD45+ cells in IPF patients, and its target gene expressions decrease in IPF BAL and lung.
(A) miR-33 relative expression in cells isolated from BAL of patients with IPF (n=62) compared to healthy controls (n=10) by Quantitative RT-PCR analysis. **(B)** miR-33 relative expression in hematopoietic cells (CD45+) isolated from IPF (n=9) compared to healthy controls (n=4). **(C)** Gene Set Variation Analysis (GSVA) of miR-33 5-p targets in BAL dataset (GSE70866), 212 IPF patients, and 20 healthy donors **(D)** Gene Set Variation Analysis (GSVA) of miR-33 5-p targets in Lung LTRC dataset (GSE47460), 254 IPF patients and 108 healthy donors. All PCR data were analyzed by non-parametric tests (Mann–Whitney *U* test or Kruskal-Wallis test where appropriate) and is presented as Mean+/-SEM. *P ≤0.05, **P <0.01, ***P<0.001, ****P<0.0001.

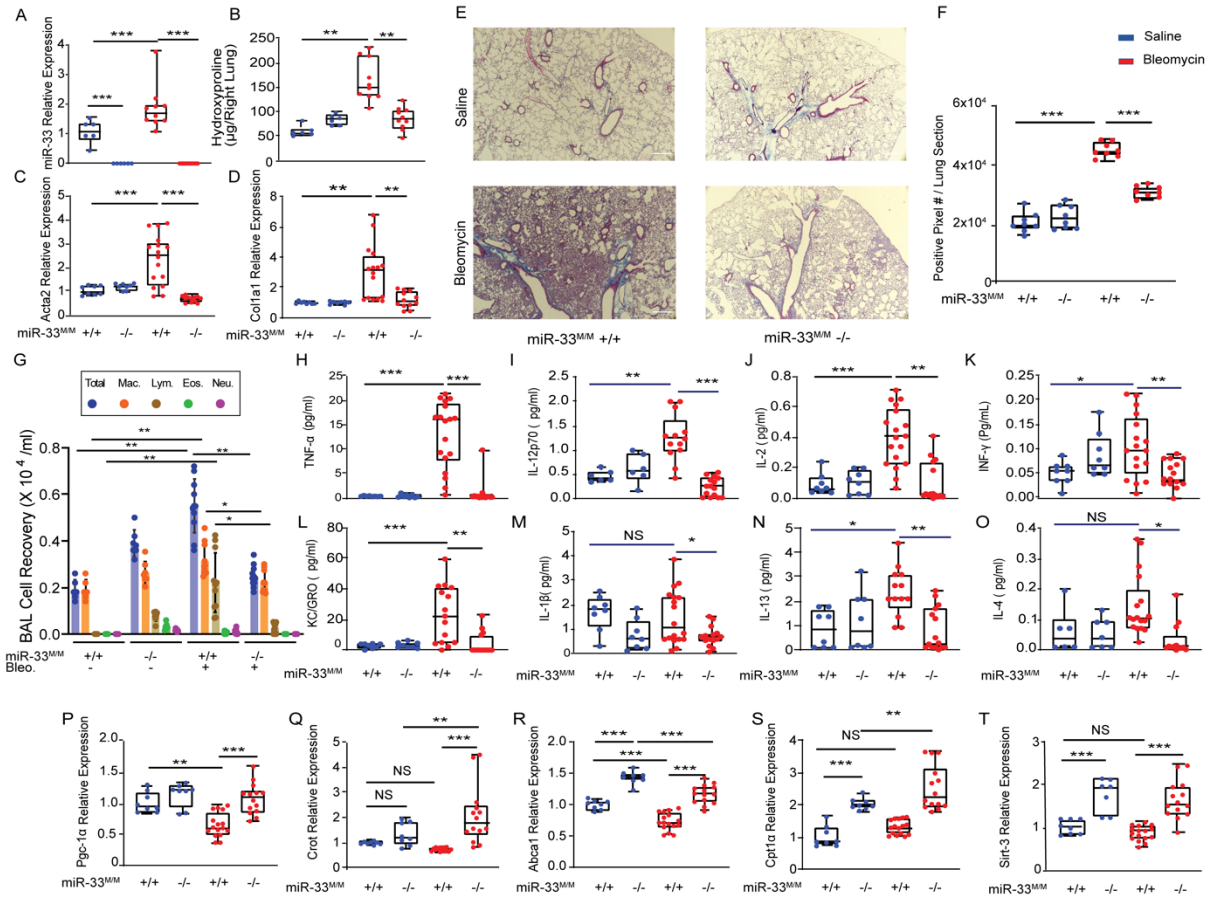

Figure 2. Loss of miR-33 in myeloid cells is protective against bleomycin-induced lung fibrosis and increases mitochondrial-related target gene expression.
Evaluation of bleomycin-induced lung fibrosis in myeloid-specific miR-33 knockout mice (*miR33$^{M/M}$-/-*) vs controls (*miR33$^{M/M}$+/+*) in bleomycin (red) compared to saline (blue) n=8 for saline and n=16 for bleomycin groups; (**A**) miR-33 relative expression by qRT-PCR analysis in AM isolated from *miR33$^{M/M}$-/-* vs controls *miR33$^{M/M}$+/+*. (**B**) Quantitative analysis of hydroxyproline in lung homogenates from indicated groups of mice. (**C, D**) *Acta2* and *col1a1* relative gene expression by qRT-PCR analysis in mice lungs from indicated groups. (**E, F**) Representative images and quantitative measurements of Masson's Trichrome staining of lung sections in *miR33$^{M/M}$-/-* vs controls *miR33$^{M/M}$+/+* with saline and bleomycin. (**G**) Differential cell counts in BAL were harvested from indicated groups. (H-O) BAL Cytokines inflammatory panel in indicated groups; (**H**) TNFα, (**I**) IL-12p70, (J) IL-2, (K) INF-γ, (L) KC, (M) IL-1β, (N) IL-13, and (**O**) Il-4. (P-T) Quantitative RT-PCR analysis of mitochondrial-related miR-33 target genes; (**P**) *Pgc-1α,* (**Q**) *Crot,* (**R**) *Abca1,* (**S**) *Cpt1α*, and (**T**) *Sirt3* in *miR33$^{M/M}$-/-* vs controls *miR33$^{M/M}$+/+* with saline and bleomycin. All data were analyzed by ANOVA or Kruskal-Wallis tests followed by posthoc analysis and is presented as Mean+/-SEM. * P ≤ 0.05, **P <0.01,

816

817

818

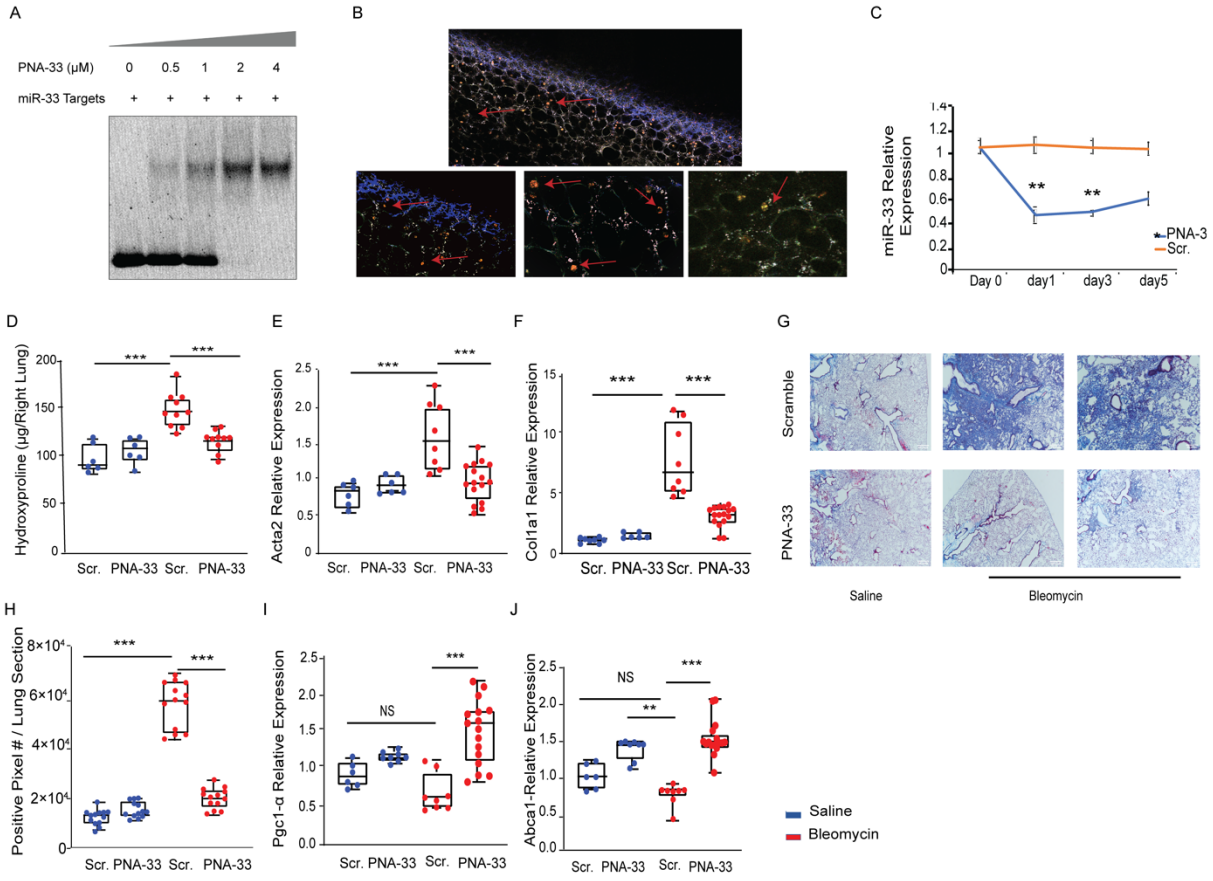

Figure 3. Pharmacological inhibition of miR-33 using PNA-33 in lung macrophages protects against bleomycin-induced pulmonary fibrosis in *in vivo* mice model of PF.
(**A**) Binding efficiency of PNA-33 to the known miR-33 targets by gel shift assay on 10% nondenaturing polyacrylamide gel. Bound and the unbound fraction of target miR-33 were visualized by staining the gel in SYBR-gold. (**B**) Two-photon microscopy imaging of PNA-33 TAMRA conjugated in WT mice 24 hours after intravenous (IV) administration, (red arrows; orange accumulation of TAMARA dye in macrophages). (**C**) miR-33 relative expression in alveolar macrophages of WT mice after intranasal (IN) administration of PNA-33 and scrambled control in different time points. (d0, d1, d3 and d5). (**D**) Quantitative analysis of hydroxyproline in lung homogenates from indicated groups of mice in Bleomycin induced lung fibrosis model. (**E, F**) *Acta2* and *Col1a1* relative gene expression by quantitative RT-PCR analysis in mice lungs from indicated groups. (**G, H**) Representative images and quantitative measurements of Masson's Trichrome staining of lung sections after administration of PNA-33/scramble control in saline and bleomycin. (**I, J**) Quantitative RT-PCR analysis of mitochondrial related miR-33 target genes; *Pgc-1α* and *Abca1* after PNA-33/ scramble control in saline and bleomycin groups. (Bleomycin; red, Saline; blue), (n=6 for saline, n=8 for bleomycin groups). All data were analyzed by ANOVA or Kruskal-Wallis tests followed by posthoc analysis and is presented as Mean+/-SEM. * P ≤ 0.05, **P <0.01, ***P<0.001.

819

820

821

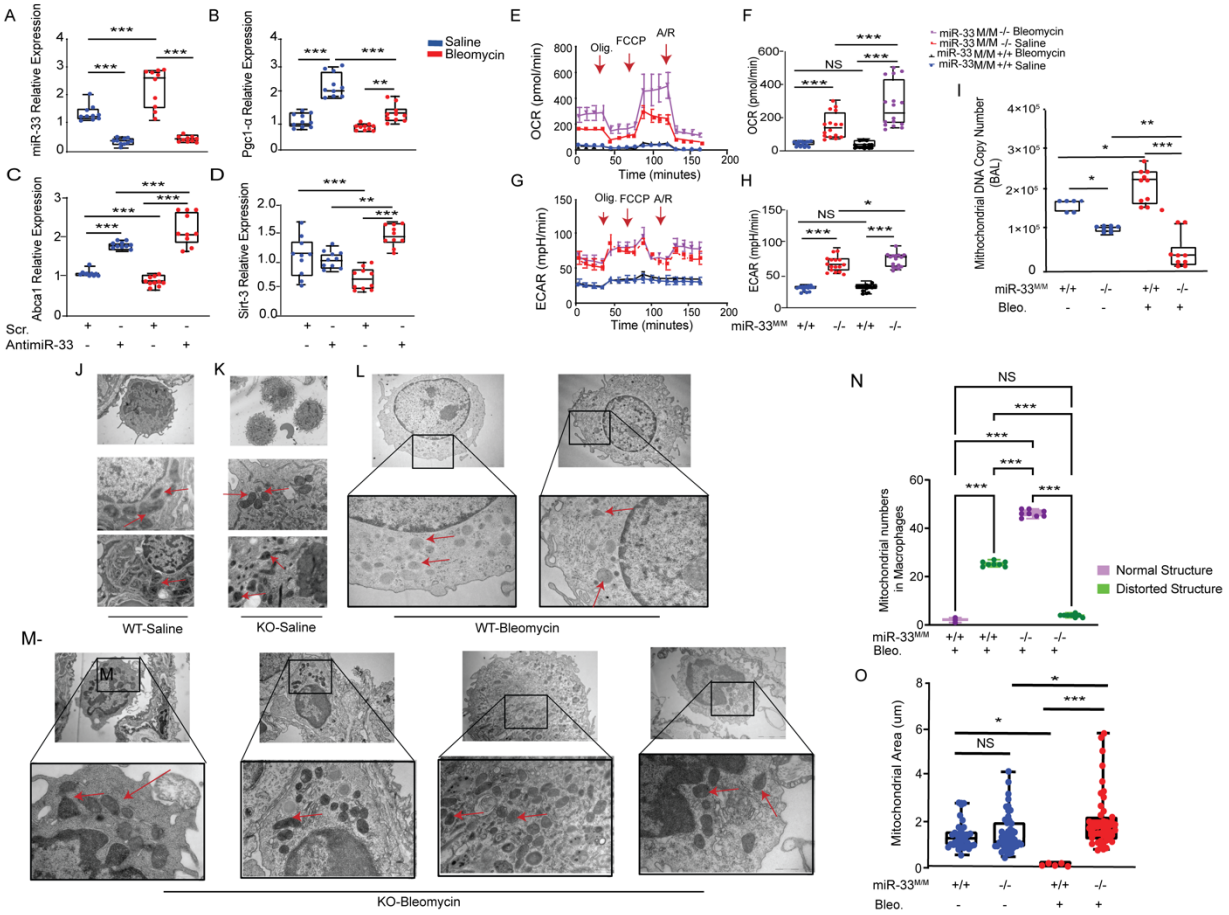

Figure 4. The absence of miR-33 in macrophages improves mitochondrial homeostasis (function and structure) at baseline and after bleomycin injury.

(**A-D**) qRT-PCR analysis of miR-33 and target gene expression in response to inhibition by miR-33 antagomir in AM *in vitro* with and without bleomycin (n=10); (**A**) miR-33, (**B**) *Pgc-1α,* (**C**) *Abca1* and (**D**) *Sirt3* relative expressions. (**E-H**) Seahorse Analysis of AM isolated from *miR33*$^{M/M}$-/- vs miR*33*$^{M/M}$+/+ in response to bleomycin and saline. The analysis was measured under basal conditions followed by the addition of oligomycin, FCCP, rotenone, and antimycin (n=16 in all groups). (**E** and **F**) Oxygen consumption rate (OCR, pmol/min), (**G** and **H**) Extracellular Acidification Rate, and (ECAR, pmpH/min). (**I**) Measurement of free circulating mitochondrial DNA (mtDNA) by Quantitative PCR in the BAL isolated from *miR33*$^{M/M}$-/- vs *miR33*$^{M/M}$+/+ mice in response to bleomycin and saline, (n=6 for saline and n=10 for bleomycin groups). (**J-M**) Representative images of Transmission Electron Microscopy (TEM) imaging on lung tissues isolated from *miR33*$^{M/M}$-/- vs *miR33*$^{M/M}$+/+ mice in response to bleomycin and saline. (n=8), red arrows are used for mitochondria. (**N**) Blinded measurements of mitochondria in TEM images from mice AM in *miR33*$^{M/M}$-/- vs *miR33*$^{M/M}$+/+ mice in bleomycin-treated mice by counting the dysmorphic versus normal-looking mitochondria in different groups (n=8). (**O**) Ultrastructural qualitative and quantitative analysis of mitochondria in mice lung TEM images represented as mitochondrial area (au) in *miR33*$^{M/M}$-/- vs *miR33*$^{M/M}$+/+ mice in bleomycin and saline-treated mice. The statistical test used were ANOVA or Kruskal-Wallis tests followed by posthoc analysis. All data is presented as Mean+/-SEM. * P ≤ 0.05, **P <0.01, ***P<0.001.

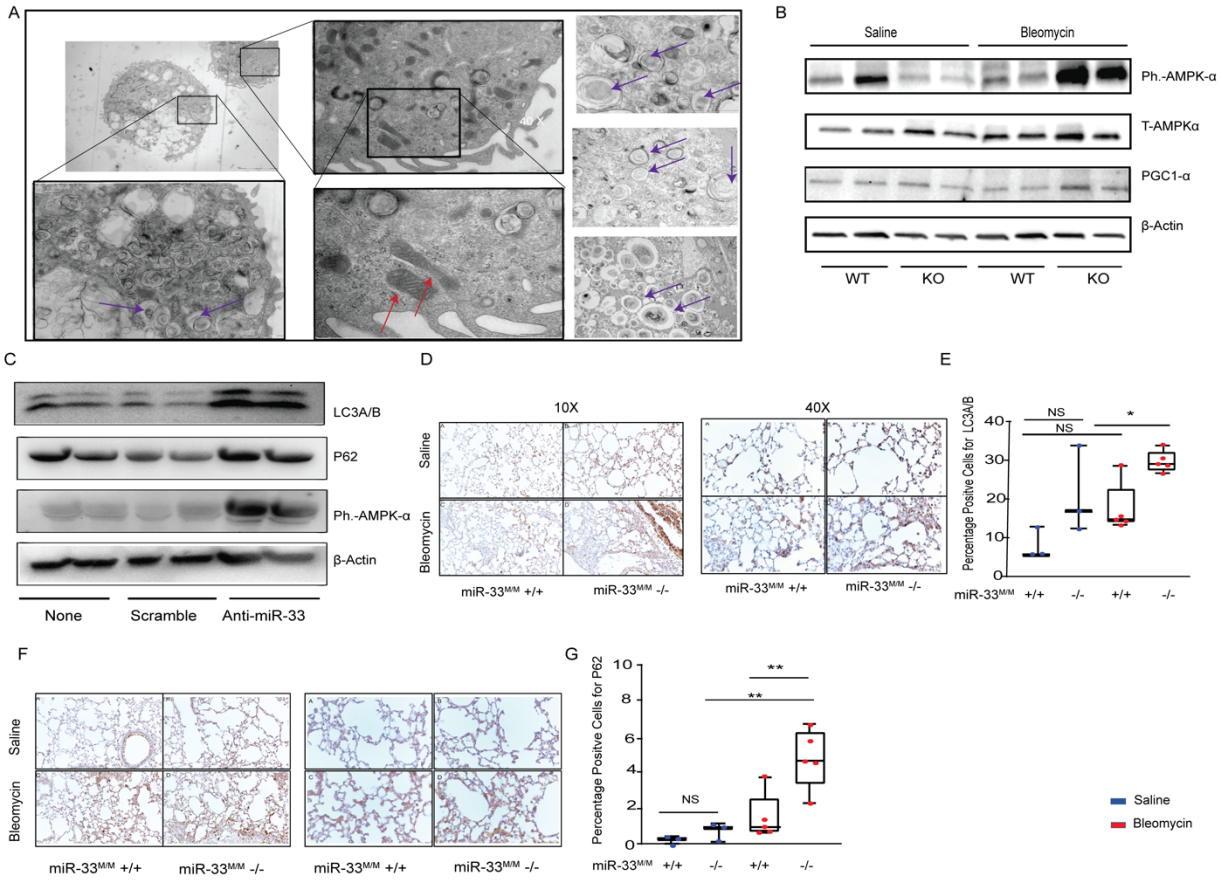

Figure 5. Genetic Ablation of miR-33 in lung macrophages induces autophagy after bleomycin injury.
(**A**) Representative images of Transmission Electron Microscopy (TEM) imaging on lung tissues isolated from *miR33*$^{M/M}$*-/-* after bleomycin. There is a dramatic increase in autophagosome contents, only in the *miR33*$^{M/M}$*-/-* macrophages after bleomycin along with the improvement in mitochondrial structure in these cells. (n=6), (red arrows for mitochondria, black arrows for autophagosome). (**B**) Western blot analysis of phospho-AMPK-α (Ph.-AMPK-α) and PGC-1α in the lung homogenates isolated from *miR33*$^{M/M}$*-/-* and controls after bleomycin and saline. (**C**) Western blot analysis of Ph.-AMPK-α, LC3A/B, and P62 in AM after inhibiting miR-33 by miR-33 antagomir. (**D**, **E**) Representative images and quantifications of Immunohistochemistry (IHC) staining of LC3A/B in lung tissues isolated from *miR33*$^{M/M}$*-/-* and controls after bleomycin and saline. (**F**, **G**) Representative images and quantifications of IHC staining of P62 in lung tissues from miR33$^{M/M}$-/- and controls after bleomycin and saline. All data were analyzed by ANOVA or Kruskal-Wallis tests followed by posthoc analysis and is presented as Mean+/-SEM. * P ≤ 0.05, **P <0.01, ***P<0.001.

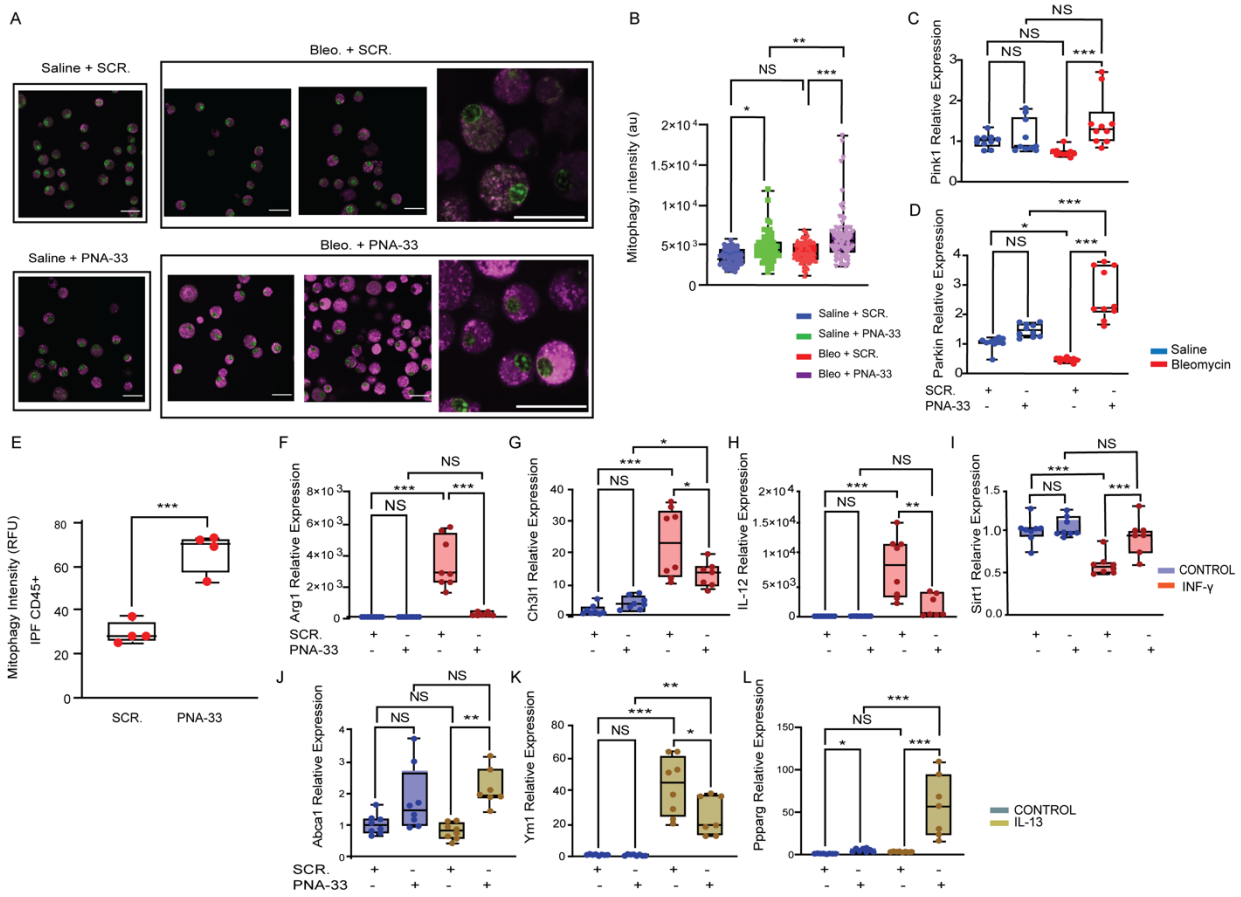

Figure 6. The absence of miR-33 in macrophages induces mitophagy in response to injury and alters cytokine-induced gene expressions in AMs.

(**A**, **B**) Mitophagy assay in primary AM isolated from WT mice treated with PNA-33 (2 nM) or scramble control after bleomycin (15nM) or saline, (**A**) Representative images in indicated groups (**B**) Quantitation of mitophagy staining. (**C**, **D**) *Pink1* and Parkin expression in PNA-33/Scramble treated primary mice AM after bleomycin/saline. (**E**) Mitophagy measurement (RFU) in CD45+ cells isolated from human IPF lungs in response to PNA-33 versus scramble control after 24 hours in culture. (n=4). (**F**-**L**) Evaluation of the effects of PNA-33/Scramble on primary mice AM after cytokines stimulation. Primary mice AM macrophages were treated with PNA-33 (2 nM) or scramble control for 24 hours before exposing them to IL-13 or INF-γ + LPS for another 24 hours. (**F**-**I**). Expression of *Arg1*, *Chi3l1*, *IL-12,* and *Sirt1* in INF-γ treated cells PNA-33/Scramble treatments. (**J**-**L**) Expressions of *Ym1*, *Abca1*, and *Pparg* in *IL-13* treated cells after PNA-33/Scramble treatments, (N=7). All data were analyzed by ANOVA or Kruskal-Wallis tests followed by posthoc analysis and data is presented as Mean+/-SEM. * $P \leq 0.05$, **P <0.01, ***P<0.001.

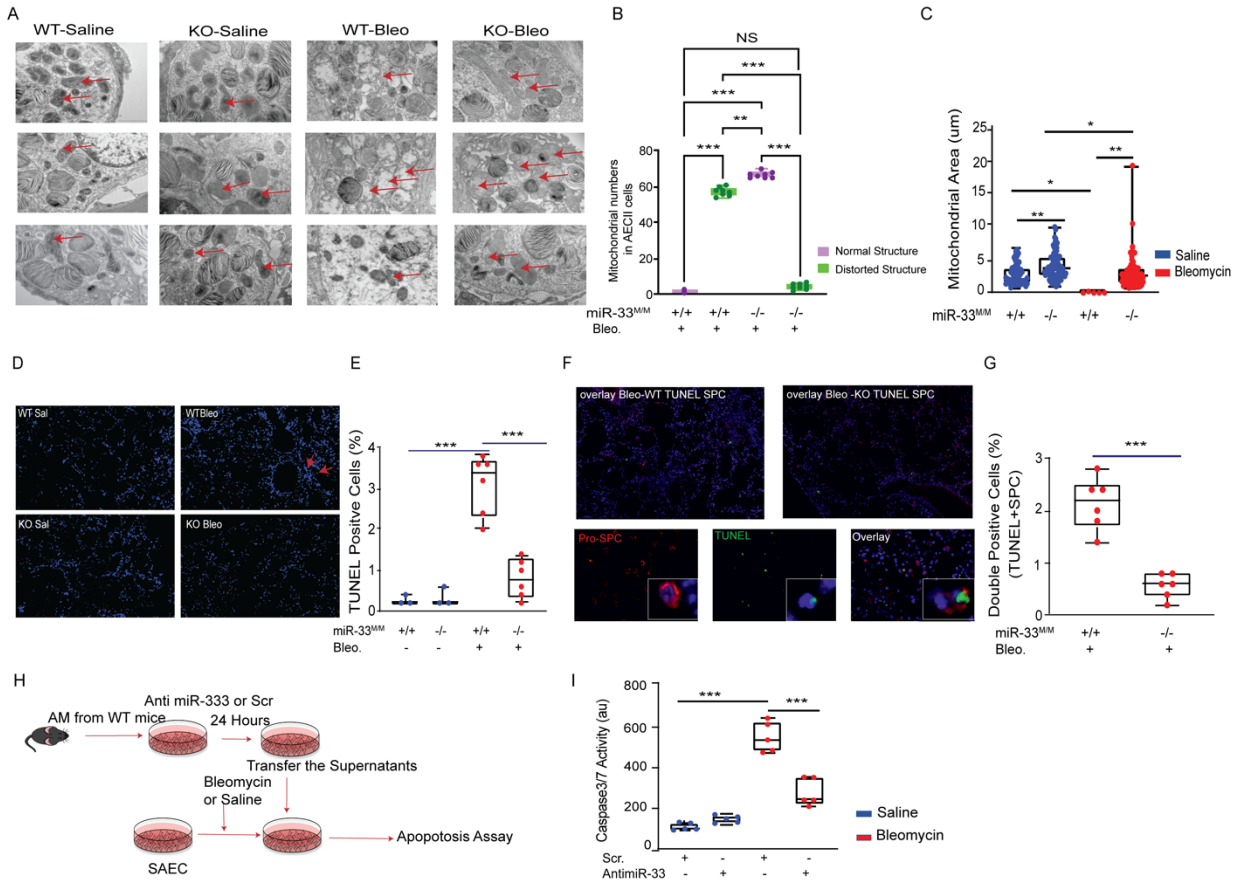

Figure 7. The absence of miR-33 in lung macrophages improves mitochondrial homeostasis and decreases cell death in Alveolar Type II cells (AECII) after bleomycin injury.

(**A**) Representative images of Transmission Electron Microscopy (TEM) on lung tissues isolated from *miR33*$^{M/M}$-/- and *miR33*$^{M/M}$+/+ after bleomycin and saline. (Red arrows are used for mitochondria in AECII cells). (n=8 per group). (**B**) Blinded measurements of mitochondria in mice AECII cells after bleomycin in TEM images by counting the dysmorphic versus normal-looking mitochondria in *miR33*$^{M/M}$-/- and control groups (n=8). (**C**) Ultrastructural qualitative and quantitative analysis of mitochondria in mice lung AECII cells in TEM images represented as mitochondrial area (au). (**D** and **E**) Representative images and quantification analysis of TUNEL IF staining on Lung sections from *miR33*$^{M/M}$-/- and *miR33*$^{M/M}$+/+ after bleomycin and Saline. (n= 6) (green: TUNEL + cells). (**F**) Representative images of TUNEL IF staining with Pro-SPC on Lung sections from *miR33*$^{M/M}$-/- and *miR33*$^{M/M}$+/+ after bleomycin (n= 6), (Green: TUNEL, Red; SPC). (**G**) Quantification analysis of double positive (TUNEL+/SPC+) cells on lung sections from *miR33*$^{M/M}$-/- and *miR33*$^{M/M}$+/+ after bleomycin. (n=6). (**H** and **I**) Schematic experimental planning of Caspase 3/7 activity measured in small airway epithelial cells (SAEC) with and without bleomycin after exposure to the supernatants harvested from ablated miR-33 AM (using PNA-33 or Scr. Control) from WT mice. All data were analyzed by ANOVA or Kruskal-Wallis tests followed by posthoc analysis and is presented as Mean+/-SEM. *P ≤ 0.05, **P <0.01, ***P<0.001.

836

837

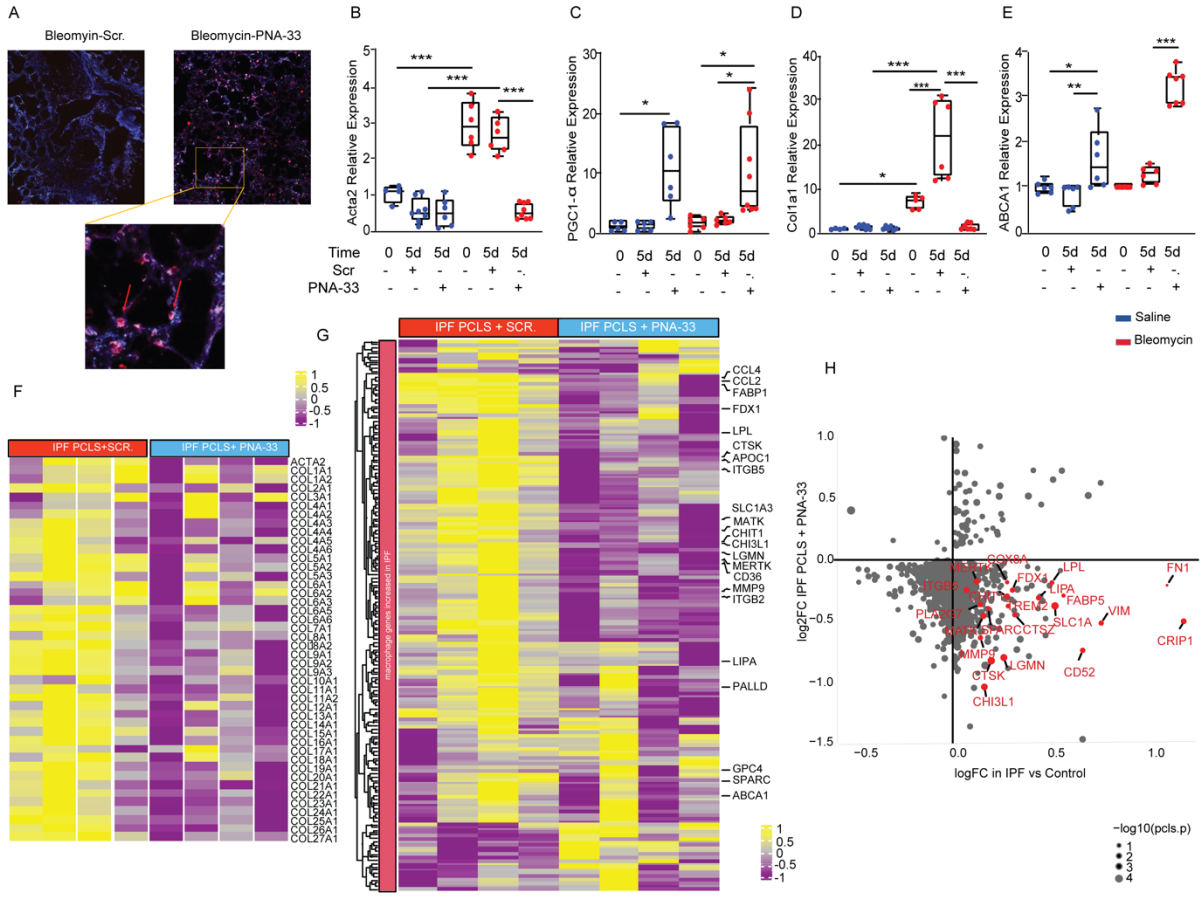

Figure 8. Pharmacologic inhibition of miR-33 using PNA-33 ameliorates fibrosis in mice and human *ex vivo* models of PF.

(**A**-**E**) Evaluation of antifibrotic effects of PNA-33 in murine *ex vivo* model. (Mice PCLS isolated at day 14 after bleomycin or saline. bleomycin; red, saline; blue). (**A**) Two-photon microscopy imaging of mice PCLS from bleomycin treated group at the end of 5 days stimulation with PNA-33 TAMRA conjugated or scramble control. (Blue; collagen, orange; TAMRA accumulation in macrophages). (**B**-**D**) qRT-PCR analysis of *Acta2, Col1a1, Pgc-1α,* and *Abca1* in mouse PCLS after bleomycin following 5 days stimulation with PNA-33 or scramble. (n=6 per group). All data were analyzed by ANOVA or Kruskal-Wallis tests followed by posthoc analysis and is presented as Mean+/-SEM. *P ≤0.05, **P <0.01, ***P<0.001. (**F**-**H**) Evaluation of antifibrotic effects of PNA-33 in human *ex vivo* model. Human precision cut lung slices (hPCLS) prepared from human IPF lungs isolated and treated with PNA-33 or scramble control for 5 days before performing RNA sequencing. (**F**) Heatmap showing the fibrotic gene expression in IPF PCLS treated with PNA-33 or scramble. (**G**) Heatmap showing the profibrotic macrophage gene expression alterations by PNA-33 in IPF PCLS. (**H**) Scatterplot of genes found significantly differentially expressed in IPF lung macrophage versus controls (in single-cell RNAseq analysis) compared with IPF PCLS treated or untreated with miR-33 inhibitor (PNA-33). The x-axis corresponds to the log fold change differences in IPF versus control lung macrophage reported in single-cell RNAseq analysis, the y-axis corresponds to fold change differences in IPF PCLS following treatment with PNA-33. The size of each dot corresponds to the negative log base-10 transformed p-values of a comparison of IPF PCLS with or without miR-33 treatment.